Electromagnetic viscosity in complex structured environments:
From blackbody to quantum friction

M. Oelschläger[1,2] D. Reiche[3,*] C. H. Egerland[1] K. Busch[1,3] and F. Intravaia[1]

[1]*Humboldt-Universität zu Berlin, Institut für Physik, AG Theoretische Optik & Photonik, 12489 Berlin, Germany*
[2]*dida Datenschmiede GmbH, Hauptstraße 8, 10827 Berlin, Germany*
[3]*Max-Born-Institut, 12489 Berlin, Germany*

We investigate the steady-state nonconservative open-system dynamics of an atom in a generic complex structured electromagnetic environment at finite temperature T. In such systems, when the atom moves along a translation-invariant axis of the environment, a frictional force acts on the particle. The effective viscosity due to friction results from the nonequilibrium interaction with the fluctuating (quantum) electromagnetic field, which effectively sets a privileged reference frame. We study the impact of both quantum and thermal fluctuations on the interaction, highlighting how they induce qualitatively different types of viscosity. To this end, we develop a self-consistent non-Markovian description that contains quantum and blackbody friction as special cases. In particular, we show how the interplay between the nonequilibrium dynamics, the quantum and the thermal properties of the radiation, as well as the confinement of light at the vacuum-material interface is responsible for several intriguing features. Our analysis is relevant for an experimental test of noncontact friction and the resulting electromagnetic viscosity.

I. INTRODUCTION

Breaking the conditions for Lorentz invariance in open quantum systems leads to a number of intriguing effects, regardless of the complexity of the system's configuration [1]. For example, in the Fulling-Davis-DeWitt-Unruh effect [2–5], an atom moving in the quantum vacuum perceives its surrounding as a thermal field when it is uniformly accelerated. When its acceleration is not uniform, as in the dynamical Casimir effect, radiation is emitted [6,7]. In such situations, an external agent is required in order to sustain the motion and to work against a drag force acting on the particle, which tends to restore the inertial dynamics [8,9]. As noted by Einstein and Hopf for a Brownian oscillator [10–12], a drag force also appears when the atom is moving with respect to a thermal field [13–16]. In this case, the nonzero-temperature part of the blackbody spectrum sets a preferred inertial frame with respect to which freely moving particles tend to have zero velocity on average. This drag force, also called blackbody friction, has been investigated in different scenarios including constant relativistic [17,18] and nonrelativistic [13,19] velocities. Its impact on the atomic linewidth-broadening [14–16] was also considered in connection with atomic clocks [20].

Another option to violate the conditions for Lorentz invariance is to introduce one or more objects in close proximity of the moving particle. In this case, even at zero temperature, a frictional force arises due to the interaction with the material-modified electromagnetic vacuum field and an external agent is required to drive the motion at constant velocity [21,22]. Due to its connection with quantum fluctuations, this drag is usually referred to as quantum friction [22]. Blackbody and quantum friction are the manifestations of a phenomenon that we call electromagnetic viscosity. Similar to classical physics [23], we quantify the viscosity in the system's steady state as

$$\mu = F/v, \tag{1}$$

where F the is total electromagnetic drag acting on the atom.

Although the viscosity has already been investigated in various contexts [16,21,24–39]—including decoherence [40], thermodynamic considerations [41,42], and its connection to Cherenkov [43] and Hawking radiation [44,45]—some interesting and relevant features have escaped attention. In the following, we generalize the earlier findings going beyond common approximations and bridging the gap between quantum and blackbody friction within a recently developed non-Markovian and self-consistent framework [44,46–48]. Within this approach we highlight the intriguing properties of the frictional interaction, recasting previous results in a more rigorous context.

The paper is structured as follows: Section II contains the central result of the present paper in the form of equivalent general expressions for the frictional force on an atom moving within a translational invariant environment. The section also contains our model and a discussion on how our formulas go beyond the existing literature. In Sec. III we analyze our expressions in detail considering a few relevant constraints. Keeping our discussion rather general, we investigate the electromagnetic viscosity in various contexts, starting with the motion of a particle in the thermal vacuum, for which we

---

*Present address: Humboldt-Universität zu Berlin, Institut für Physik, AG Optical Metrology & Joint Lab Integrated Quantum Sensors, 12489 Berlin, Germany; reiche@physik.hu-berlin.de
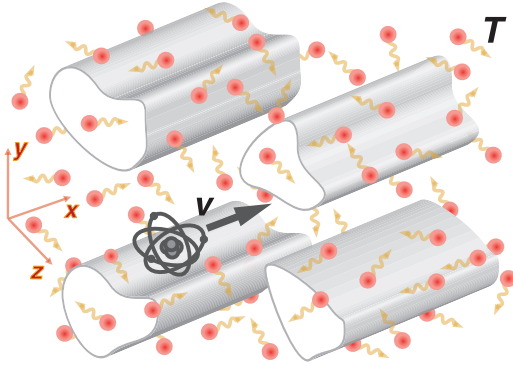
FIG. 1. Schematic of an atom moving parallel to an arrangement of different, translationally invariant objects surrounded by thermal radiation at temperature T.

assess the validity of a common approximation. We show that at finite temperature and at small velocity, the electromagnetic viscosity necessarily scales as $\propto v^0 T^2$ for a large class of substances which includes typical materials. It also naturally decomposes into three contributions

$$\mu \to \mu_T = \mu_T^{\text{vac}} + \mu_T^t + \mu_T^r. \quad (2)$$

Here, (i) μ_T^{vac} describes the interaction with the thermal quantum vacuum field, (ii) μ_T^t includes the interaction between the material-modified field and the atomic translational degrees of freedom, and (iii) μ_T^r corresponds to the contribution involving the exchange of angular momentum. The latter arises from the so-called spin-momentum locking of light [49,50], a behavior induced by the natural confinement of the electromagnetic field in the vicinity of an interface of two different materials [51]. As we will see, μ_T^r tends to reduce the frictional interaction and its description requires the inclusion of the full backaction from the environment onto the dynamics of the particle. This contribution is therefore not covered by traditional approximate or equilibrium-based techniques. Our analysis allows us to identify well-defined scales which characterize in which regimes thermal or quantum fluctuations dominate the frictional interaction. At the end of this section, we test our general results addressing, as an example, the specific geometry of a plate for which we provide detailed analytical asymptotes as well as numerical evaluations [52]. In Sec. IV, we analyze our findings from a different perspective and explore the spectral density of the interaction between atom and field. Finally, in Sec. V, we close our discussion with summarizing remarks.

II. DIPOLE FORCE ON A MOVING ATOM

We consider an electrically neutral atom that is propelled by an external agent along the x direction, corresponding to the direction of translational invariance of a complex macroscopic electromagnetic environment (see Fig. 1). The environment is structured by N (not necessarily identical) translationally invariant objects comprised of common, linear, and passive material(s). For simplicity, we neglect magnetic properties of both the atom and its surroundings. The atom's motion (its center-of-mass kinematics) is assumed to be described by the classical trajectory $\mathbf{r}_a(t) = x_a(t)\mathbf{x} + \mathbf{R}_a$. This

is usually a good approximation as long as we consider atoms with relatively large masses or velocities (de Broglie wavelengths less than one angstrom). The position of the atom in the transversal plane $\mathbf{R}_a \equiv (y_a, z_a)$ is assumed to be constant. Practically, this might be resulting from the specific structuring of the environment (e.g., a geometry-material configuration that neutralizes transversal forces on the atom [53]), external interactions (e.g., external potentials [54,55]), or in general from considering configurations where the change $\mathbf{R}_a \equiv (y_a, z_a)$ might be neglected with respect to the relevant timescales.

During its motion, due to the interaction with the electromagnetic field, the atom experiences a drag force which, after some transient dynamics, eventually balances the external drive. The focus of our analysis is on the investigation and characterization of the viscosity when the system reaches this nonequilibrium steady state (NESS), i.e., when the atom moves at constant velocity $\mathbf{v} = v\mathbf{x}$. In our description, we assume that the total system's density matrix at the initial time t_0 in the far past of the experiment factorizes into $\hat{\rho}(t_0) = \hat{\rho}_{\text{atom}}(t_0) \otimes \hat{\rho}_{\text{field}}(t_0)$. In the NESS, however, due to its dissipative nature, the total system does not conserve any memory of its initial condition. We also consider geometric dimensions such that a dipole description of the particle is sufficient and we can neglect higher-order multipoles. The atom is then described by its electric-dipole operator $\hat{\mathbf{d}}$ and the total electric field by the operator $\hat{\mathbf{E}}$. In our case, the electric field which would exist without the atom, $\hat{\mathbf{E}}_0$, is supposed to be thermalized at temperature T and, therefore, obeys the fluctuation-dissipation theorem [56]. In momentum and frequency space, we can write

$$\left\langle \hat{\mathbf{E}}_0(q, \mathbf{R}_a, \omega)\hat{\mathbf{E}}_0^{\mathsf{T}}(\tilde{q}, \mathbf{R}_a, \tilde{\omega}) \right\rangle$$
$$= 8\pi^2 \hbar [1 + n(\omega)] \underline{G}_\Im(q, \mathbf{R}_a, \omega)\delta(\omega + \tilde{\omega})\delta(q + \tilde{q}), \quad (3)$$

where q is the component of the wave vector along the x direction, ω is the frequency of the radiation, $\hbar$ is Planck's reduced constant and $\delta(\cdot)$ is the Dirac function. The superscript "T" gives the transpose of a matrix rendering the previous product of operators a dyadic (see Appendix). $\underline{G}$ is the Green tensor that solves Maxwell's equations with appropriate boundary conditions for our setup. Since we will be interested in positions having the same transversal coordinates, $\mathbf{R}_a$ will appear only once in the argument of the Green tensor. The angular brackets denote the quantum average over the initial state density matrix $\hat{\rho}(t_0)$, the subscript "$\Im$" denotes a specific form of the tensor, which for the Green tensor is $\underline{G}_\Im = (\underline{G} - \underline{G}^\dagger)/(2i)$. Also, we have defined the Bose occupation number $n(\omega) = (e^{\beta\hbar\omega} - 1)^{-1}$ with the inverse temperature $\beta = 1/(k_B T)$ and where k_B is Boltzmann's constant.

Some general comments can be made about the tensor $\underline{G}_\Im$ [48,57]: In vacuum, due to the transversality of the field, $\underline{G}_\Im$ is a symmetric tensor and is even in q. However, in the vicinity of an interface, due to the spatial confinement characterizing the near field, the radiation can feature a longitudinal component with respect to the direction of motion. This translates into (off-diagonal) skew-symmetric components in $\underline{G}_\Im$ that are odd in q. Mathematically, this encodes the so-called spin-momentum-locking of light [58]. As we see below, the

latter has specific consequences in our particular context [see discussion after Eq. (20)].

In the nonrelativistic case, the motion-induced drag experienced by the atom can be written as

$$F(t) = \lim_{\mathbf{r} \to \mathbf{r}_a(t)} \langle \hat{\mathbf{d}}(t) \cdot \partial_x \hat{\mathbf{E}}(\mathbf{r}, t) \rangle, \tag{4}$$

which is related to the x component of the Lorentz force [51,59]. For our purposes it is convenient to decompose the electric-field operator as a sum of $\hat{\mathbf{E}}_0$, the uncoupled field introduced above, and $\hat{\mathbf{E}}_{\text{ind}}$ which describes the radiation induced by the atom. Proceeding as in Ref. [46], we can write

$$\hat{\mathbf{E}}_{\text{ind}}(\mathbf{r}, t) = \int_{t_0}^{t} dt' \underline{G}(\mathbf{r}, \mathbf{r}_a(t'), t - t') \hat{\mathbf{d}}(t')$$

$$= 2i \int_0^{t-t_0} d\tau \int \frac{d\omega}{2\pi} \int \frac{dq}{2\pi} e^{-i\omega\tau} e^{iq[x - x_a(t-\tau)]}$$

$$\times \underline{G}_\Im(q, \mathbf{R}_a, \omega) \hat{\mathbf{d}}(t - \tau) \quad (\tau = t - t'). \tag{5}$$

Given that the interaction between the atomic internal degrees of freedom and the electromagnetic fluctuations is typically weak, we focus on linear dynamics for the dipole operator associated with a single frequency ω_a, corresponding to the transition from the highest occupied orbital to the lowest unoccupied one. We can hence model the particle in terms of a three-dimensional (3D) isotropic oscillator [59,60]

$$(\partial_t^2 + \omega_a^2) \hat{\mathbf{d}}(t) = \alpha_0 \omega_a^2 \hat{\mathbf{E}}(\mathbf{r}_a(t), t), \tag{6}$$

where α_0 is the static atomic polarizability, describing the coupling between the atom and the electromagnetic radiation [46,51,59].

When the NESS is achieved, we have that $x_a(t) \sim vt$. Then, we can solve the system self-consistently up to all orders in the coupling (connected to α_0 [48]) and evaluate the atomic power spectrum $\underline{S}_v(\omega)$ from the dipole correlator [48,51] $\langle \hat{\mathbf{d}}(\omega) \hat{\mathbf{d}}^\mathsf{T}(\tilde{\omega}) \rangle = 4\pi^2 \delta(\omega + \tilde{\omega}) \underline{S}_v(\omega)$, obtaining

$$\underline{S}_v(\omega) = \underline{\alpha}_v(\omega) \underline{\kappa}_v(\omega) \underline{\alpha}_v^\dagger(\omega). \tag{7a}$$

The extra subscript "v" explicitly denotes that the expressions are evaluated in the NESS and, therefore, depend on the velocity. The tensors $\underline{\kappa}_v$ and $\underline{\alpha}_v$ are, respectively, the steady-state nonequilibrium electric field's power spectrum [Eq. (3)] and the steady-state dressed atomic polarizability. They can be written as

$$\underline{\kappa}_v(\omega) = \frac{\hbar}{\pi} \int \frac{d\tilde{q}}{2\pi} [n(\omega_{\tilde{q}}^+) + 1] \underline{G}_\Im(\tilde{q}, \mathbf{R}_a, \omega_{\tilde{q}}^+), \tag{7b}$$

$$\underline{\alpha}_v(\omega) = \left[\mathbb{1} - \alpha_{\text{B}}(\omega) \int \frac{dq}{2\pi} \underline{G}(q, \mathbf{R}_a, \omega_q^+) \right]^{-1} \alpha_{\text{B}}(\omega), \tag{7c}$$

where $\omega_q^\pm = \omega \pm qv$ is the Doppler-shifted frequency, $\mathbb{1}$ is the three-dimensional unit matrix, and $\alpha_{\text{B}}(\omega) = \alpha_0 \omega_a^2 / (\omega_a^2 - [\omega + i0^+]^2)$ is the (causal) bare polarizability of the isolated atom [61]. The appearance of the Green tensor in Eq. (7c) indicates that the polarizability is dressed via the interaction with the electromagnetic environment.

A. Three equivalent expressions describing the frictional interaction

For our next step it is useful to rewrite the expression in Eq. (4) as follows:

$$F(t) = \lim_{\mathbf{r} \to \mathbf{r}_a(t)} 2\text{Re}\langle \hat{\mathbf{d}}(t) \cdot \partial_x \hat{\mathbf{E}}^\oplus(\mathbf{r}, t) \rangle, \tag{8}$$

where $\hat{\mathbf{E}}^\oplus$ is the positive-frequency component of the electric-field operator (we refer to Ref. [47] for details). While the order of the operators is irrelevant in Eq. (4), notice that this is not true anymore for the above rewritten version, Eq. (8). As a consequence the specific ordering of Eq. (8) has to be preserved in the calculation. It is well known that, despite that the final result is independent from this choice, the interpretation of the different contributions appearing in the final expression and their attribution to the dipole or the field dynamics might depend on it [47,62,63]. Inserting our description for the dipole's and the field's dynamics [Eqs. (5)–(7)] in Eq. (8) yields in the steady-state ($-t_0, t \to \infty$) the frictional force (see the Appendix)

$$F = -2 \int_0^\infty d\omega \int \frac{dq}{2\pi} q \, \text{Tr}\left[\left\{ \frac{\hbar}{\pi} n(\omega) \underline{\alpha}_{v,\Im}(-\omega_q^-) \right. \right.$$

$$\left. \left. + \, \underline{S}_v(-\omega_q^-) \right\} \underline{G}_\Im^\mathsf{T}(q, \mathbf{R}_a, \omega) \right], \tag{9}$$

where we have defined $\underline{\alpha}_{v,\Im}$ analogously to $\underline{G}_\Im$ and we have used that $\underline{G}_\Im(q, \mathbf{R}_a, \omega) = -\underline{G}_\Im^\mathsf{T}(-q, \mathbf{R}_a, -\omega)$ as well as the fact that the product of a symmetric and a skew-symmetric matrix vanishes under the trace. In Eq. (9), the first and the second term in the curly brackets, respectively, correspond to the dipole interacting with the unperturbed field $\hat{\mathbf{E}}_0$ and the induced field $\hat{\mathbf{E}}_{\text{ind}}$. We note that both terms depend on the temperature [the power spectrum implicitly via the nonequilibrium fluctuation-dissipation theorem in Eq. (7a)]. Equation (9) generalizes the expression for the frictional force reported in previous work [47,59] for $T \neq 0$ and includes both blackbody and quantum friction as special limits. The latter is recovered noticing that $n(\omega) \to 0$ for $T \to 0$ ($\omega > 0$), while the former requires the use of the vacuum Green tensor and some further considerations (see below). It is opportune to mention here that the previous calculation explicitly uses the assumption of a linear relation between the dipole's and the electric field's dynamics. This is, for example, the case for the isotropic oscillator described in Eq. (6). Conversely, the procedure leading to the zero-temperature version of Eq. (9) does not depend on the concrete model that describes the atomic internal degrees of freedom [47,59].

The physics of the system imprints some mathematical properties on the quantities appearing in Eq. (9). These can be used to rewrite the above expression in a different but equivalent form. Indeed, replacing $\omega \to \omega + qv$ and realizing that the integral kernel is an odd function on the interval $q \in (-\infty, \infty)$ and $\omega \in [-qv, 0]$, we can rewrite Eq. (9) as

$$F = 2 \int_0^\infty d\omega \int \frac{dq}{2\pi} q \, \text{Tr}\left[\left\{ \frac{\hbar}{\pi} [1 + n(\omega_q^+)] \underline{\alpha}_{v,\Im}(\omega) \right. \right.$$

$$\left. \left. - \, \underline{S}_v(\omega) \right\} \underline{G}_\Im(q, \mathbf{R}_a, \omega_q^+) \right]. \tag{10}$$

Here, we have also utilized that $n(-\omega) = -[1 + n(\omega)]$, $\underline{\alpha}_{v,\Im}(-\omega) = -\underline{\alpha}_{v,\Im}^{\mathsf{T}}(\omega)$ and that the power spectrum fulfills the identity $\underline{S}_v(-\omega) = \underline{S}_v^{\mathsf{T}}(\omega) - (\hbar/\pi)\underline{\alpha}_{v,\Im}^{\mathsf{T}}(\omega)$ (see the Appendix for details). The main difference between Eqs. (9) and (10) lies in a rearrangement of the contributions due to the field's and to the dipole's dynamics. In particular, Eq. (10) corresponds to an approach where the splitting related to a positive and negative frequency integration is not performed (see the Appendix).

We can recast the expression for the frictional force in a third equivalent form. Considering Eq. (7a), we can write the following alternative expression:

$$
\begin{aligned}
F = \frac{\hbar}{\pi} \int_0^\infty d\omega \int \frac{dq}{2\pi} q \int \frac{d\tilde{q}}{2\pi} \\
\times \left\{ \coth\left(\frac{\beta\hbar\omega_q^+}{2}\right) - \coth\left(\frac{\beta\hbar\omega_{\tilde{q}}^+}{2}\right) \right\} \\
\times \operatorname{Tr}[\underline{\alpha}_v(\omega)\underline{G}_\Im(\tilde{q}, \mathbf{R}_a, \omega_{\tilde{q}}^+)\underline{\alpha}_v^\dagger(\omega)\underline{G}_\Im(q, \mathbf{R}_a, \omega_q^+)], \quad (11)
\end{aligned}
$$

where we used that $2n(x) = \coth(x/2) - 1$. To derive the previous equation we used that $\underline{\alpha}_{v,\Im}$ is connected to the Green tensor via the identity

$$
\underline{\alpha}_{v,\Im}(\omega) = \underline{\alpha}_v(\omega) \int \frac{dq}{2\pi} \underline{G}_\Im(q, \mathbf{R}_a, \omega_q^+)\underline{\alpha}_v^\dagger(\omega). \quad (12)
$$

Equation (11) is the result we would have obtained avoiding the frequency splitting and using the symmetric ordering for the operators (see the Appendix). The advantage of the previous equation is that it explicitly manifests the quadratic behavior of the frictional interaction in the Green tensor, revealing thereby the strong nonadditive features already observed in the zero-temperature case [53]. This means that also for $T \neq 0$ a modification of the geometry or materials of the setup leads to a nontrivial change of the viscosity coefficients [45,53,64].

Equations (9)–(11) provide three equivalent expressions describing the electromagnetic drag acting on an atom moving within a translational invariant environment. In view of these alternative expressions, it becomes manifest that, as expected, the corresponding ordering of operators, when carried out consistently, has no consequences for the observable force.

B. Comments and general considerations

The previous expressions bear some similarities with other results existing in the literature [16,21,28,29,31–33,41]. However, they feature important differences and go beyond many standard approximations. Our approach is nonperturbative and fully non-Markovian. It avoids issues which have been pointed out in earlier work showing the necessity of an adequate bookkeeping of all contributions within a perturbative approach [65] and the need for a good description of the system's low frequency (long time) behavior [45,47]. It also dispenses with common assumptions used by equilibrium-based techniques. One of the most common is the local thermal equilibrium (LTE) approximation, which forgoes the opportunity to solve the system exactly and directly applies the equilibrium fluctuation-dissipation theorem also to evaluate nonequilibrium correlators. In the LTE approximation, spatially separated but interacting subsystems (e.g., in our

case the atom and the field) are assumed to be at equilibrium, although the whole system is out of equilibrium [21]. Technically, in our case, it amounts to replacing $n(\omega_{\tilde{q}}^+) \to n(\omega)$ in Eq. (7b) (see Refs. [47,48] for details) or equivalently $\coth(\beta\hbar\omega_{\tilde{q}}^+/2) \to \coth(\beta\hbar\omega/2)$ in Eq. (11). Depending on the system, the validity of this approach is questionable [48] and it was already disproved for quantum friction [46,51]. It was shown that this approximation ignores certain low-frequency contributions to the power spectrum of the interaction [48]. The generalization provided by Eqs. (9), (10), or (11) allows us to extend our considerations to finite temperature and to assess the validity of the approximation. In the following, we will often use the LTE approximation as a reference in order to highlight the difference introduced by our nonequilibrium theory in the description of the electromagnetic viscosity at finite temperature.

Another relevant aspect of our approach is that is allows us to investigate a part of the interaction involving the spin of the radiation at finite temperature. This contribution was recently analyzed in the case of quantum friction and here we treat the finite temperature generalization. In the case of quantum friction, it was shown how it deeply affects the interaction and allows us to tune it [51,53]. Mathematically, the spin-dependent component of the interaction is encoded in the tensorial structure of the integral kernels of all the expressions for the drag given above. The key quantities are the dressed polarizability and the power spectrum in Eqs. (7). In particular, Eq. (7a) is central because it generalizes the nonequilibrium fluctuation-dissipation theorem introduced in previous work [46,51] to finite temperatures: In spite of its formal resemblance to equilibrium fluctuation-dissipation theorems [56], Eq. (7a) not only allows us to go beyond the LTE approximation but also includes effects that do not subsist in equilibrium. Equations (7) reveal that the particle's power spectrum is deeply intertwined with the electromagnetic environment (represented by the Green tensors), highlighting the importance of a self-consistent approach that fully includes backaction from the field onto the particle [19,48]. More precisely, the behavior of dressed polarizability *and* the field spectrum in Eqs. (7) can be related to the electromagnetic local density of states through the diagonal part of the Green tensor, $\rho_{\mathrm{LDOS}} \propto \operatorname{ImTr}[\underline{G}]$ [66]. Interestingly, however, the tensorial structure of the expression for the force indicates that off-diagonal elements of the Green tensor can also contribute to the interaction. These off-diagonal elements are connected to the spin local density of states introduced in Ref. [45,51] and specifically to the spin-momentum locking of light in the vicinity of a surface [67], which describes a well-defined connection occurring between the spin and the wave vector of the electromagnetic radiation. In combination with the occurring of Doppler-shifted frequencies, the light-matter interaction then conveys a transfer of momentum which depends on the exchange of angular momentum between the atom and the field. This generates a corresponding component for the force [51], whose behavior will become an important part in our discussion of μ_T [see Eq. (26)].

In the next sections we analyze in detail our results in some limiting cases. We further discuss their connections as well as their differences with respect to the existing literature

and highlight the new information achievable within our more comprehensive description.

III. THERMAL AND QUANTUM VISCOSITY

We now turn our attention back to our main result, specifically to Eq. (11), and focus on the behavior of the viscosity coefficient μ [see Eq. (1)]. In the following (see Secs. III A and III B), we focus first on the behavior of μ at the leading order in the velocity, since the corresponding expressions are more likely to be relevant in experiments. The behavior of the drag at higher velocities as well as the corresponding velocity scales are discussed at the end of Sec. III C. Subsequently, we consider the concrete example of an atom moving parallel to a flat interface (see Sec. III D).

A. Viscosity at low velocities: Motion through the thermal vacuum

Let us consider Eq. (11) and the corresponding viscosity coefficient μ [see the definition in Eq. (1)]. Expanding the coth functions to linear order in v, we obtain an electromagnetic viscosity coefficient which only depends on the temperature and $\mathbf{R}_a$, i.e.

$$
\mu_T \sim -\frac{\hbar^2 \beta}{2\pi} \int_0^\infty d\omega \int \frac{dq}{2\pi} \int \frac{d\tilde{q}}{2\pi} \frac{q(q-\tilde{q})}{\sinh^2\left(\frac{\beta\hbar\omega}{2}\right)}
$$
$$
\times \mathrm{Tr}[\underline{\alpha}_{v=0}(\omega)\underline{G}_{\Im}(\tilde{q},\mathbf{R}_a,\omega)\underline{\alpha}^\dagger_{v=0}(\omega)\underline{G}_{\Im}(q,\mathbf{R}_a,\omega)]. \tag{13}
$$

We start with a remark about the case of an atom moving through thermal vacuum. Since the vacuum Green tensor is symmetric and even in q (or $\tilde{q}$) [68], the term $\propto q\tilde{q}$ in Eq. (13) vanishes under the integration over the wave vectors. We also have that

$$
\int \frac{dq}{2\pi} q^2 \mathrm{Tr}[\underline{G}_{\Im}(q, \mathrm{R}_a, \omega)] = \frac{\omega^5}{6\pi\epsilon_0 c^5}, \tag{14}
$$

with ϵ_0 being the vacuum permittivity [68]. Since vacuum is homogeneous and isotropic, taking Eq. (7c) into account, we further find that $\underline{\alpha}_{v,\Im}(\omega) = \mathrm{Im}[\alpha_{v=0}(\omega)]\underline{\mathbb{1}}$. Therefore, Eq. (13) reduces to

$$
\mu_T^{\mathrm{vac}} \sim -\frac{v\hbar^2\beta}{3\pi c^5(4\pi\epsilon_0)} \int_0^\infty d\omega \, \mathrm{Im}[\alpha_{v=0}(\omega)] \frac{\omega^5}{\sinh^2\left(\frac{\beta\hbar\omega}{2}\right)}. \tag{15}
$$

This is the result for blackbody friction obtained in Ref. [13] and by others later [14–16,18,20,41].

For the sake of completeness, we quickly review the main outcomes surrounding the result in Eq. (15), postponing a more general discussion related with our approach to Sec. IV. The frictional force vanishes in the limit $T \to 0$, corresponding, as expected, to a viscosity μ_T^{vac} which is exclusively thermal. Depending on the temperature or more precisely on the thermal frequency $\omega_{\mathrm{th}} = k_B T/\hbar$, the main contribution to the integral in Eq. (15) is characterized either by the frequency range which includes the atomic transition, $\omega_{\mathrm{th}} \gtrsim \omega_a$, or not, $\omega_{\mathrm{th}} < \omega_a$. In the first case, on can approximate $\mathrm{Im}[\alpha_{v=0}(\omega)] \sim \mathrm{Im}[\alpha_B(\omega)] = \alpha_0\omega_a\pi\delta(\omega_a - \omega)/2$ ($\omega > 0$) leading to the vac-

uum thermal viscosity

$$
\mu_T^{\mathrm{vac}} \sim -\frac{\alpha_0}{4\pi\epsilon_0} \frac{\hbar\omega_a^5}{3c^5} \frac{\beta\hbar\omega_a}{\sinh^2\left(\frac{\beta\hbar\omega_a}{2}\right)}. \tag{16}
$$

For optical transitions, however, such a behavior occurs at the rather high temperatures of $\approx 10^4$ K. At smaller temperatures, $k_B T \ll \hbar\omega_a$, Eq. (16) does not represent the correct expression since low frequencies dominate the integrand in Eq. (13). The approximation we used to describe the polarizability for computing Eq. (16) is no longer adequate and we need to employ the dressed polarizability. Upon inserting the vacuum Green tensor [68] in Eq. (7c), we obtain at the leading order of the atom-surface coupling

$$
\mu_T^{\mathrm{vac}} \sim -\frac{32\pi^5}{135}\hbar\frac{\alpha_0^2}{\epsilon_0^2}\left(\frac{k_B T}{\hbar c}\right)^8, \quad k_B T \ll \hbar\omega_a, \tag{17}
$$

which replaces the exponentially damped result from Eq. (16).

Equation (17) is one example of incorporating higher-order corrections of the atom-field coupling into the description and a similar expression was discussed earlier in the context of one-loop corrections to the quantum-electrodynamical atom-field coupling [16,18]. In our approach, the corresponding expressions arise naturally from the self-consistent description of light-matter interaction, which in Eq. (15) results in a particle's optical response that is fully dressed. Notice also that many of the earlier works derived μ_T^{vac} in Eq. (15) using the LTE approximation. At first sight, this might appear in contrast with our discussion at the end of the previous section about the formalism that led to Eq. (15). Interestingly, however, at the leading order in the velocity, considering the LTE approximation in Eq. (11), i.e., $\coth(\beta\hbar\omega_{\tilde{q}}^+/2) \to \coth(\beta\hbar\omega/2)$, is mathematically identical to neglecting the $\propto q\tilde{q}$ term in Eq. (13). In other words, for the motion-induced electromagnetic viscosity acting on an atom in a vacuum at finite temperature, our nonequilibrium framework predicts that deviations from the LTE approximation appear at orders higher than linear in v. This result further clarifies the role of the LTE in the frictional interaction and helps to avoid possible sources of confusion.

B. Viscosity at low velocities: Motion through a structured environment

Equation (13) becomes more interesting when the atom's environment is no longer homogeneous, i.e., when, in addition to the thermal field, other macroscopic objects are present in the space near the atom. In this case, the Green tensor is not necessarily symmetric [57,69] and the previous considerations made for vacuum do not apply. Still, since the Green tensor is a susceptibility [70], $\underline{G}_{\Im}(q, \mathbf{R}_a, \omega)$ is odd in ω and, consistently with Eq. (5), one also has $\underline{G}_{\Im}(q, \mathbf{R}_a, 0) = 0$. For simplicity, in the following, we additionally assume that all the translationally invariant objects comprising the electromagnetic environment are made from an (not necessarily local and not necessarily the same) "Ohmic material." For our analyses, this assumption is mathematically equivalent to the requirement $\underline{G}'_{\Im}(q, \mathbf{R}_a, 0) \neq 0$, where the prime denotes a derivative with respect to frequency. This property applies to a large class of dissipative and dispersive materials.

Generalizations are possible and, as an example, we refer to Ref. [71] where the frictional interaction at zero temperature between an atom and lossy multilayer structures is discussed.

Inspecting Eq. (13) [or also Eq. (10)], one realizes that the thermal field relevantly impacts the interaction at frequencies $\omega \lesssim \omega_{\text{th}}$. At room temperature, this yields $\omega_{\text{th}} \approx 26$ meV (about 0.34 meV at 4 K) which is much smaller than typical optical transition frequencies of, e.g., alkali-metal atoms [72] or resonances of common materials [73]. For our purposes it is then reasonable to assume that the temperature cannot appreciably excite any resonance in the system. As for Eq. (17), our interest lies in the frequency regime $\omega_{\text{th}} < \omega_a$, which provides the leading-order correction to the zero-temperature result. This can be found by considering the moment asymptotic expansion [74,75]

$$\frac{\hbar\beta}{2\sinh^2\left(\frac{\beta\hbar\omega}{2}\right)} \sim -2\delta(\omega) + \frac{\pi^2}{3}\frac{2}{\hbar^2\beta^2}\delta''(\omega), \qquad (18)$$

where the double-prime denotes the second derivative with respect to frequency. The first term corresponds to the zero-temperature limit while the second term is the first thermal correction. Upon inserting the above expression into Eq. (13), we find, however, that the expression arising from the first term on the right-hand side (r.h.s.) of Eq. (18) always identically vanishes due to the properties of the Green tensor. In other words, in the steady-state, we always have $\lim_{T\to 0}\mu_T = 0$, which is equivalent to saying that at zero temperature the frictional force does not have a linear dependence in velocity [29,40,76]. In empty space, this can be understood as a consequence of the system's Lorentz invariance. When material interfaces are present, this result is less evident and has been discussed elsewhere [30,59,77,78]. In agreement with some earlier work [40,47,53,59,65], it indicates that in the steady state at $T = 0$, when only quantum fluctuations are present, we would have to expand the frictional force in Eq. (11) to higher orders in v to have a nonzero electromagnetic viscosity. In particular, in the steady-state for the Ohmic case, quantum friction corresponds at the leading order in the velocity to the electromagnetic viscosity $\mu(v, 0) = \mu_{\text{QF}} \propto v^2$. The latter has been previously analyzed [51,53] and for completeness we report the result for μ_{QF} at leading order in the atom-surface coupling,

$$\mu_{\text{QF}} \sim -\frac{\alpha_0^2 \hbar v^2}{12\pi}\int\frac{dq}{2\pi}\int\frac{d\tilde{q}}{2\pi}(q+\tilde{q})^4$$
$$\times \text{Tr}[\underline{G}'_{\Im}(\tilde{q}, \mathbf{R}_a, 0)\underline{G}'_{\Im}(q, \mathbf{R}_a, 0)]. \qquad (19)$$

We recall that the previous expression is the result of an analysis showing that quantum friction at low velocities is typically a low-frequency phenomenon, dominated by $\omega \lesssim v/\lambda_a$, where λ_a usually correspond to the minimal distance from one of the objects shaping the electromagnetic environment of the atom. We remark that for Eq. (19) it was assumed that v/λ_a is much smaller than any of the system's resonance frequencies (note that for $v \approx 1$ km/s and $\lambda_a \approx 1$ nm, one has $v/\lambda_a \approx 0.6$ meV [46,53]).

The second term on the r.h.s. of Eq. (18) gives the leading-order temperature correction of the low-velocity electromagnetic viscosity in Eq. (13). Independently from the geometry and the detailed material composition of the envi-

ronment, our approach shows that the temperature correction scales quadratically in T and corresponds to a frictional force that grows linearly with v in the steady state. This is in line with other analyses, where specific geometries and materials have been considered [21,29,40,76,79]. Focusing on the leading order in atom-surface coupling, using the symmetries of the integral kernel with respect to the wave vector as well as that $\underline{G}_{\Im}$ is odd with respect to frequency, the temperature correction can be written in a form which is similar to Eq. (19), i.e.,

$$\mu_T \sim -\frac{\alpha_0^2\pi}{3\hbar\beta^2}\int\frac{dq}{2\pi}\int\frac{d\tilde{q}}{2\pi}(q-\tilde{q})^2$$
$$\times \text{Tr}[\underline{G}'_{\Im}(\tilde{q}, \mathbf{R}_a, 0)\underline{G}'_{\Im}(q, \mathbf{R}_a, 0)]. \qquad (20)$$

The previous equation represents an additional central result of this paper. Since $\underline{G}_{\Im}(q, \mathbf{R}_a, \omega)$ is a Hermitian positive-semidefinite tensor (for $\omega > 0$), Eq. (20) implies that, in general, $\mu_{\text{QF}}, \mu_T \leqslant 0$ as one should expect for a frictional force. Also, for a generic (passive) system that is translationally invariant along the x axis, $\underline{G}_{\Im}(q, \mathbf{R}_a, \omega)$ can be written in terms of a real, symmetric (positive-semidefinite) matrix $\underline{\Sigma}(q, \mathbf{R}_a, \omega)$ (even in q) and a real vector $\mathbf{s}_\perp(q, \mathbf{R}_a, \omega)$ (odd in q) normal to the invariance axis [80]. We have indeed that

$$\underline{G}_{\Im}(q, \mathbf{R}_a, \omega) = \underline{\Sigma}(q, \mathbf{R}_a, \omega) + \mathbf{s}_\perp(q, \mathbf{R}_a, \omega) \cdot \underline{\mathbf{L}}, \qquad (21)$$

where $[\underline{L}_i]_{jk} = -i\epsilon_{ijk}$. denotes the generator of 3D rotations around the i axis [see also discussion below Eq. (3)] [53]. The vector $\mathbf{s}_\perp(q, \mathbf{R}_a, \omega)$ is connected to the spin-dependent part of the electromagnetic density of states. In addition, using the properties of the trace, Eq. (21) leads to the decomposition

$$\mu_T = \mu_T^t + \mu_T^r. \qquad (22)$$

The first term contains only the symmetric matrix, $\underline{\Sigma}$:

$$\mu_T^t \sim -\alpha_0^2\frac{2\pi}{3\hbar\beta^2}\int\frac{dq}{2\pi}\int\frac{d\tilde{q}}{2\pi}q^2$$
$$\times \text{Tr}[\underline{\Sigma}'(\tilde{q}, \mathbf{R}_a, 0)\underline{\Sigma}'(q, \mathbf{R}_a, 0)], \qquad (23)$$

and, since $\underline{\Sigma}$ is positive semidefinite, we have that, in Eq. (23), $\mu_T^t < 0$. The previous expression can be related to the description of the thermal correction of the electromagnetic viscosity, which is usually obtained within the LTE approximation. Hence, the term μ_T^r is not captured within the LTE approach, while it is in ours. Using $\text{Tr}[\underline{L}_i\underline{L}_j] = 2\delta_{ij}$, μ_T^r reads

$$\mu_T^r \sim \alpha_0^2\frac{4\pi}{3\hbar\beta^2}\int\frac{dq}{2\pi}\int\frac{d\tilde{q}}{2\pi}q\tilde{q}\mathbf{s}'_\perp(\tilde{q}, \mathbf{R}_a, 0)\cdot\mathbf{s}'_\perp(q, \mathbf{R}_a, 0)$$
$$= \alpha_0^2\frac{4\pi}{3\hbar\beta^2}\left\|\int\frac{dq}{2\pi}q\mathbf{s}'_\perp(q, \mathbf{R}_a, 0)\right\|^2. \qquad (24)$$

As mentioned above, it is connected to the interaction between atom and electromagnetic excitation with nonzero spin. Its role has already been highlighted for quantum friction [51], i.e., strictly $T = 0$, whereas we consider here the finite-temperature case. Interestingly, like for the zero-temperature limit, the previous analysis shows that μ_T^r is positive and, therefore, tends to decrease the viscosity experienced by the moving atom [e.g., see Eq. (26) below]. In combination with the spin-momentum locking, this reduction can be related to a transfer of momentum to the atom from the field which is

selectively mediated through an exchange and a net transfer of angular momentum [51]. Given its physical origin, in complete analogy with the $T = 0$ case [53], the impact of μ_T^r can be diminished by choosing an axis-symmetric geometry that, for a trajectory along the symmetry axis, suppresses the exchange of angular momentum between the atom and the radiation. Indeed, for symmetry reasons, along such a trajectory, one must have $\mathbf{s}_\perp = 0$.

C. Viscosity regimes and characteristic scales

Lastly, we would like to point out that, while $\mu_T \to \mu_T^{\mathrm{vac}} \propto T^8$ in Eq. (17) is related to the general properties of vacuum, the quadratic temperature dependence of μ_T in Eq. (20) is connected to the presence of objects and our Ohmic assumption on the electromagnetic response of the involved materials. This is also equivalent to a local density of states that scales linearly with the frequency for $\omega \to 0$. Deviations from the Ohmic behavior, including those leading to μ_T^{vac}, are contained in our theory, but more quantitative estimations require us to adequately reconsider Eq. (13) and its low-frequency limit. Mathematically, these features are encoded in the Green tensor $\underline{G}$. In particular, the expected transition $\mu_T \propto T^2 \to T^8$ as a function of the distance of the atom from the objects can be seen as a consequence of the general decomposition $\underline{G} = \underline{G}_0 + \underline{G}_{\mathrm{sc}}$. Here, $\underline{G}_0$ is the homogeneous vacuum Green tensor and $\underline{G}_{\mathrm{sc}}$ is the scattering part of the Green tensor, due to the presence of the objects [31]. The two tensors not only scale differently with the frequency but also with $\mathbf{R}_a$: while $\underline{G}_0$ does not depend on $\mathbf{R}_a$ and is always nonzero, the contribution of $\underline{G}_{\mathrm{sc}}$ scales as the inverse of the distance between the atom to the objects' surface ($\approx \lambda_a$), making the scattering contribution more or less relevant as a function of $\mathbf{R}_a$.

Some general considerations can also be made regarding the transition $\mu_{\mathrm{QF}} \leftrightarrow \mu_T \propto T^2$ and the behavior of μ at higher velocities. As discussed above, the viscosity coefficients are connected with the low-frequency behavior of the integrand in Eq. (11). The two characteristic frequency scales are, respectively, v/λ_a and $k_{\mathrm{B}}T/\hbar$. They are related to the hyperbolic cotangents appearing in Eq. (11), which effectively limit the range of the frequency integration. In the Ohmic limit, we have $\mu_{\mathrm{QF}} \gtrsim \mu_T$ if $v/\lambda_a \gtrsim k_{\mathrm{B}}T/\hbar$ and vice versa. This allows us to define the following critical velocity, distance, and temperature:

$$v_c \approx \frac{k_{\mathrm{B}}T\lambda_a}{\hbar}, \quad \lambda_c \approx \frac{\hbar v}{k_{\mathrm{B}}T}, \quad T_c \approx \frac{\hbar v}{k_{\mathrm{B}}\lambda_a}. \quad (25)$$

They determine the characteristic scales where μ_{QF} and μ_T interchange their role as the dominant contribution to the interaction, emphasizing which kind of phenomenon (thermal vs quantum fluctuations) is mainly responsible for the breaking the conditions for Lorentz invariance. Curiously, the atom needs to have a sufficiently high kinetic energy ($v > v_c$) to start to capture more of the "quantumness" of the frictional force (at $T = 3$ K and for $\lambda_a \approx 10$ nm one has that $v_c \approx 4$ km/s). Indeed, for $v < v_c$, the electromagnetic viscosity is essentially given by μ_T. Physically, this behavior can be understood by considering the different mechanisms in the frictional process. As for blackbody friction, it is the thermal bath that nonresonantly drives the interaction at low
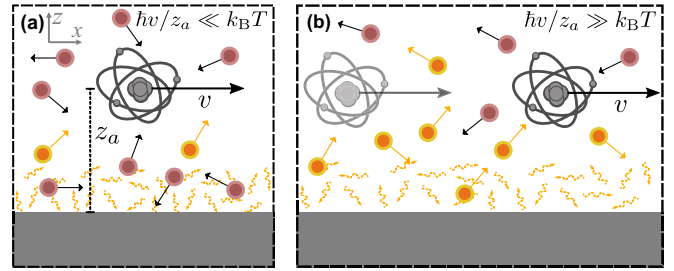

FIG. 2. Schematic description of the different mechanisms determining the viscosity perceived by an atom moving in a complex structured electromagnetic environment. (a) At sufficiently low velocities, large distances or high temperatures, the frictional process is dominated by thermal excitations (red points with black arrows). (b) At high velocities, short separations or low temperatures, the system behaves more according to its quantum characteristics: The viscous dynamics is determined by the interactions with the electromagnetic quantum fluctuations. Due to the anomalous Doppler effect, the atom can get excited (not shown) and virtual excitations can become real (yellow points with yellow arrows) at the expense of the kinetic energy of the atom. The relevance of these excitations "extracted" from vacuum grows with v and dominates over the thermal interaction at sufficiently high velocities. In both limits, the local electromagnetic density of states is modified by the presence of the vacuum-material interface (yellow curly arrows), inducing a functional dependence of the frictional interaction on the atom-surface separation.

velocity [see Fig. 2(a)]. However, due to the boundary conditions imposed by the nonhomogeneity of the environment, the density of states for the electromagnetic field is substantially different from that of the empty space, specifically in the evanescent region due the appearance of surface states. The difference in the density of state induces a modification in the interaction which depends on the position of the atom (see also Sec. IV below). Simultaneously, however, due to the motion-induced anomalous Doppler effect [51,81–83], the atom can get excited and *virtual* excitations (surface polaritons) can be "energized" and become *real* at the expense of the atomic kinetic energy, participating in the frictional process [see Fig. 2(b)]. Their relevance is proportional to the velocity of the atom and connected to the shape of the density of states of the electromagnetic field, determining the functional dependency in v of μ_{QF}. Therefore, for constant T, depending on v, either the quantum or the thermal mechanism dominates the frictional interaction.

The same frequency scales v/λ_a and $k_{\mathrm{B}}T/\hbar$ allow us to understand the behavior of the viscosity at higher velocity. As we already saw with blackbody friction, as soon as the integration range includes the atomic resonance ω_a, the behavior of the viscosity changes and its value is likely enhanced. In this case, one can speak of a resonant interaction where the thermal radiation or the virtual excitations which have become real have sufficient energy to excite the atomic transition and drive the absorption and the emission process at the leading order (single-excitation level). Still, due to the broadband nature of the involved electromagnetic field, the interaction usually remains weak despite the enhancement. We can, in general, define the threshold temperature $T \approx T_a \equiv \hbar\omega_a/k_{\mathrm{B}}$

and velocity $v_a \equiv \omega_a \lambda_a$ above which this behavior occurs. While $T_a \approx 10^4$ K for optical transitions, v_a can be diminished by shortening the distance of the particle from the surface of one of the objects in the environment. Still, for $\lambda_a \approx 1$ nm and optical transitions, one has that v_a is at the order of $\approx 10^{-2}$ the speed of light, which is larger than typical values in experiments and justifies our analysis for low velocities. Conversely, as previously pointed out for specific configurations [16,65] and confirmed within our general framework, at velocities and temperatures smaller than v_a and T_a, the interaction is nonresonant and one needs to consider higher-order (two- or more-excitation-) processes in order to correctly describe the frictional dynamics. Interestingly, these observations can be more generally connected to the nature of the available (dissipative) interaction channels within the system. We will cover this topic with more detail in Sec. IV.

D. Example: An atom moving at constant height and velocity above a flat surface

To illustrate our general findings in more detail, it is instructive to consider a simple and widely used setup to compute the viscosity coefficients, i.e., an atom moving in vacuum at constant velocity with respect to a single planar half space located at $z \leqslant 0$ and comprised from a local, Ohmic, dispersive, and dissipative material. In this case $z_a = \lambda_a$ measures the distance from the bulk's interface. For simplicity, we focus here on a motion in the near field of the surface since this is the regime where the frictional interaction becomes most relevant [21]. Upon inserting the corresponding expression for the Green tensor [47,51,68] and performing the wave-vector integrals, we find [79,84,85]

$$\mu_T = -\frac{3}{\pi} \hbar \alpha_0^2 \rho^2 \frac{\left(\frac{k_B T}{\hbar}\right)^2}{(2 z_a)^8}, \quad \mu_T^r = -\frac{\mu_T^t}{2}, \quad (26)$$

where $\rho = \lim_{\omega \to 0} \partial_\omega \mathrm{Im}[r(\omega)]/(2\epsilon_0)$ with $r(\omega)$ being the transverse magnetic Fresnel coefficient. The parameter ρ, which is connected to the low-frequency tail of the local density of states, highlights the dissipative properties of the electromagnetic environment and, specifically for conductors, effectively corresponds to the resistivity of the involved material. Notice that, since it is connected with our assumption of an Ohmic behavior, the limit $\rho \to 0$ in the previous expression has to be handled with care and in general does not imply the vanishing of the electromagnetic viscosity. We already saw that, when ρ vanishes because no objects are present ($\underline{G}_{\mathrm{sc}} \to 0$), Eq. (26) needs to be replaced by Eqs. (16) and (17). For non-Ohmic materials, Eq. (26) needs to be reevaluated. For example, in the limit of a nondissipative material with a constant and real refraction index n, the frictional interaction is occurring above the Cherenkov threshold, i.e., $v \gtrsim c/n$ [83,86]. In the specific geometry considered here, we find that the spin-sensitive part of the interaction turns out to reduce the viscosity by a factor of one half. For comparison, for the same setup, the electromagnetic viscosity exclusively due to quantum fluctuations is also given by $\mu_{\mathrm{QF}} = \mu_{\mathrm{QF}}^t + \mu_{\mathrm{QF}}^r$, where

$$\mu_{\mathrm{QF}} = -\frac{18}{\pi^3} \hbar \alpha_0^2 \rho^2 \frac{v^2}{(2 z_a)^{10}}, \quad \mu_{\mathrm{QF}}^r = -\frac{5}{7} \mu_{\mathrm{QF}}^t. \quad (27)$$

This corresponds to a reduction of μ_{QF}^t by roughly 70% due to μ_{QF}^r [51]. As discussed above, the contribution associated with μ^r can be suppressed in specific geometries, independently from the temperature. In Ref. [53] it was pointed out that this suppression further enhances the nonadditive behavior of the electromagnetic viscosity. Specifically, when the atom moves close enough to N objects (see Fig. 1), the resulting total viscosity μ^N has a maximal enhancement with respect to a single interface μ^{surf} which roughly scales as $\mu^N/\mu^{\mathrm{surf}} \approx \phi N^2$. Based on the previous arguments, one should expect $\phi_{\mathrm{QF}} \approx (1 - 5/7)^{-1} = 7/2$ when μ_{QF} dominates or $\phi_T \approx (1 - 1/2)^{-1} = 2$ when μ_T describes the frictional process. According to this estimate, for an atom moving at the center of a cavity made from two identical metallic parallel plates ($N = 2$), it was previously shown that $\mu_{\mathrm{QF}}^{\mathrm{cav}}/\mu_{\mathrm{QF}}^{\mathrm{surf}} \approx 17$ [53]. Similarly, at finite temperature, using Eq. (20), one obtains $\mu_T^{\mathrm{cav}}/\mu_T^{\mathrm{surf}} \approx 12$.

Defining the reduced thermal wavelength $\lambda_{\mathrm{th}} = c/\omega_{\mathrm{th}} = \hbar c/(k_B T)$ (≈ 7.6 μm at 300 K) and $\lambda_\rho = 4\pi\epsilon_0 c\rho$, the expressions given in Eqs. (17), (26), and (27) allow for a direct assessment of the different contributions to the viscosity coefficient in the low-velocity nonresonant limit. In particular, by looking at the ratios μ_T/μ_{QF} and $\mu_T^{\mathrm{vac}}/\mu_T$, we can precisely characterize the transition from quantum friction to the thermal behavior given by μ_T and additionally from μ_T to blackbody friction. For the atom-plate configuration, the transition $\mu_{\mathrm{QF}} \leftrightarrow \mu_T$ of the electromagnetic viscosity is described by the quantities

$$v_c \equiv \sqrt{\frac{2}{3}} \pi \frac{z_a}{\lambda_{\mathrm{th}}} c, \quad \lambda_c \equiv \sqrt{\frac{3}{2\pi^2}} \frac{v}{c} \lambda_{\mathrm{th}}, \quad T_c \equiv \sqrt{\frac{3}{2\pi^2}} \frac{\hbar v}{k_B z_a}, \quad (28a)$$

which are a refinement of those given in Eq. (25), confirming our general predictions. The additional characteristic scales for $\mu_T \to \mu_T^{\mathrm{vac}}$, addressing the transition to black-body friction, can be given as

$$\ell_c \equiv \frac{\sqrt{2}}{4} \left[\sqrt{\frac{5}{2}} \frac{\lambda_\rho}{\lambda_{\mathrm{th}}} \right]^{\frac{1}{4}} \frac{c}{v} \lambda_c, \quad \mathcal{T}_c \equiv \frac{1}{4} \left(\frac{\sqrt{15}}{2\pi} \frac{\lambda_\rho}{z_a} \right)^{\frac{1}{3}} \frac{c}{v} T_c. \quad (28b)$$

We illustrate these findings in Figs. 3–6, where we compare the numerical evaluation of the full expression for $\mu = F/v$ [see e.g., Eq. (11)] with the asymptotic behavior given above. As shown in Fig. 3, the quantum frictional interaction starts to be relevant for the drag force acting on the particles only when $v > v_c$. At lower velocities the viscosity is instead characterized by μ_T (for sufficiently small distance we can neglect the impact of blackbody friction). At sufficiently high velocities ($v \gtrsim v_a \equiv \omega_a z_a$) the frictional interaction enters the resonant regime, where $\mu(v)$ suddenly increases with v [47] (see also Sec. IV).

In Fig. 4, we depict the electromagnetic viscosity μ at constant velocity and temperature as a function of the distance z_a of the atom from the interface with the material. As expected, the quantum frictional force dominates for $z_a < \lambda_c$. In the proximity of macroscopic surfaces comprised of common (dissipative) materials, both the viscosities μ_T and μ_T^{vac} are usually subleading. At separations larger than λ_c, the viscosity
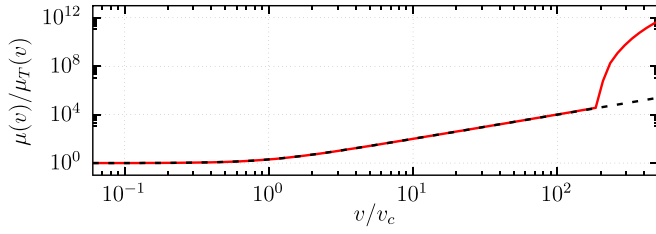
FIG. 3. Electromagnetic viscosity $\mu = F/v$ acting on an atom moving near a surface as a function of the velocity v for constant temperature $T = 3$ K and distance $z_a = 5$ nm. For the atom we chose $\alpha_0 = 4\pi\epsilon_0 \times 47.28$ Å^3 and $\omega_a = 1.6$ eV (corresponding to a ^{87}Rb atom) [72]. The surface is described by a Drude-permittivity $\epsilon(\omega) = 1 - \omega_p^2/[\omega(\omega + i\Gamma)]$ using the parameters $\omega_p = 7.36$ eV, $\Gamma = 202$ meV (corresponding to lead [87,88]), giving $\rho = \Gamma/[\epsilon_0\omega_p^2] = 277$ nΩ m and $\lambda_\rho \approx 9.24$ nm. The function $\mu(v)$ (full red line) is normalized with respect to the asymptotic expression for μ_T given in Eq. (26). At low velocity $v < v_c$ [$v_c \approx 5$ km/s in this case, see Eq. (28)], the viscosity is characterized by its thermal behavior, which for the chosen parameters is dominated by μ_T. For $v > v_c$, the quantum component becomes relevant and the interaction behaves as $\mu_{QF} \propto v^2$. The dashed black line describes the nonresonant asymptotic behavior according to Eqs. (26) and (27). At sufficiently high velocities, the viscosity enters the resonant regime, visible as a sudden rise of the viscosity as a function of v ($v_a = \omega_a z_a \approx 2.41 \times 10^3 v_c$ for the chosen parameters—see also Sec. IV).

connected to μ_T becomes relevant, while the effect of the distance-independent blackbody friction occurs for $z_a > \ell_c$, where $\mu_T^{vac}/\mu_T > 1$. In Fig. 5, a similar behavior is visible as a function of the temperature. For $T < T_c$, the viscosity is dominated by the quantum fluctuations, while the thermal effects appear at $T > T_c$, where $\mu(T) \sim \mu_T \propto T^2$. At a higher temperature $T \gtrsim T_a \equiv \hbar\omega_a/k_B$, the interaction becomes resonant and grows faster with T (see Sec. IV). In the nonresonant regime blackbody friction would become relevant for $T > \mathcal{T}_c$.
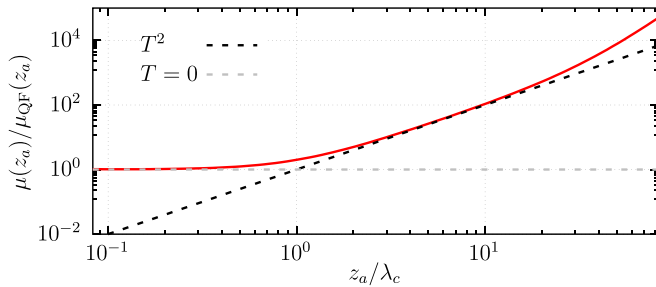

FIG. 4. Electromagnetic viscosity of an atom moving near a planar interface. The atom and the surface are described in terms of the same parameters used in Fig. 3. The plot depicts $\mu = F/v$ [full red line, see e.g., Eq. (9)] as a function of the distance z_a at a constant temperature $T = 3$ K and velocity $v = 12$ km/s ($\lambda_c \approx 12$ nm). The viscosity is normalized with respect to the asymptotic expression μ_{QF} given in Eq. (27). At separations $z_a/\lambda_c < 1$ the drag is essentially due to quantum friction (horizontal dashed gray line). At distances $z_a/\lambda_c > 1$, the electromagnetic viscosity $\mu_T \propto T^2$ becomes dominant (black dashed line). Blackbody friction starts to be relevant at separations $z_a/\ell_c > 1$ ($\ell_c/\lambda_c \approx 584$ for the parameters given above).
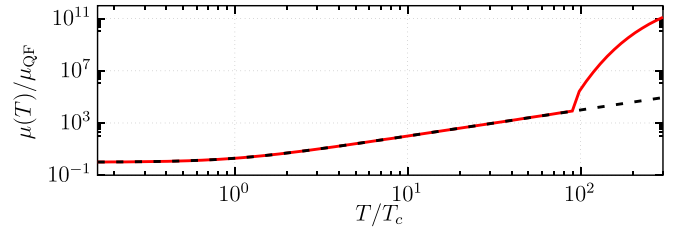

FIG. 5. The viscosity μ as a function of the temperature for an atom moving near a planar surface. The atom and the material parameters are the same as in Fig. 3. The velocity and the distance from the surface are kept constant: $v = 12$ km/s and $z_a = 5$ nm, leading to the value $T_c = 7.14$ K. The value of $\mu(T)$ (full red line) is normalized with respect to μ_{QF} given in Eq. (27). The dashed black line describes the asymptotic behavior according to Eqs. (26) and (27). At $T < T_c$, the frictional interaction is dominated by the quantum fluctuations of the system, while at higher temperatures it becomes more thermal and the viscosity is described by μ_T. For temperatures $T \gtrsim T_a$ ($\approx 2.6 \times 10^3 T_c$ for the corresponding values), the interaction becomes resonant and is characterized by a strong increase as a function of temperature (see Sec. IV). Given that $\mathcal{T}_c/T_c \approx 6.5 \times 10^3$ for this specific case, blackbody friction is always subleading in the nonresonant regime.
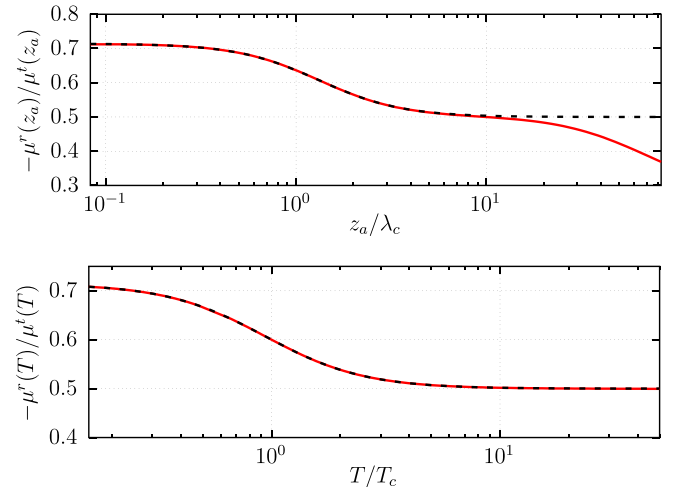

FIG. 6. Relative behavior of the electromagnetic viscosity components μ^r and μ^t as a function of the atom-surfaces separation (top) and the temperature (bottom). In the upper plot the temperature is set to $T = 3$ K and in the lower plot the distance is $z_a = 5$ nm. In both cases the velocity is $v = 12$ km/s. The atom and the surface are described in terms of the same parameters used in Fig. 3. The plot shows that a transition from $-\mu^r/\mu^t \sim 5/7$ to $-\mu^r/\mu^t \sim 1/2$ occurs around the characteristic distance $z_a \approx \lambda_c$ (top) and temperature $T \approx T_c$ (bottom). For $z_a \approx \ell_c$, the viscosity enters the regime where μ_T^{vac} becomes dominant. For these distances μ^r goes to zero and, given that $\ell_c = 584\lambda_c$ for the above parameters, a decreasing of $-\mu^r/\mu^t$ is expected. As a function of the temperature, the transition to blackbody friction would instead occur around $T \approx \mathcal{T}_c \approx 6.5 \times 10^3 T_c$. The dashed black lines describe the asymptotic behavior predicted according to Eqs. (26) and (27), where the contribution of blackbody friction was neglected.
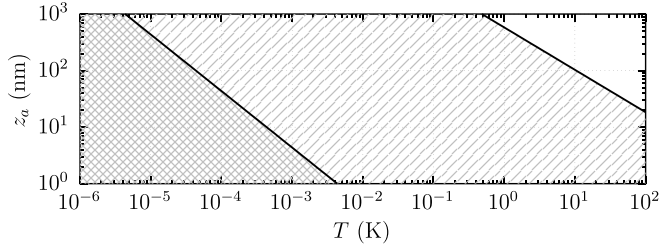
FIG. 7. Physical character of the electromagnetic viscosity at constant velocity as a function of distance z_a and temperature T. We can clearly distinguish three regimes. (i) For small separations or small temperatures (lower-left corner of the plot) the quantum frictional viscosity $\mu \sim \mu_{\rm QF}$ and the system's quantum behavior dominates the frictional interaction. (ii) At $z_a T \gtrsim \sqrt{3/2}\hbar v/(k_{\rm B}\pi)$, the thermal fluctuations from the material interface μ_T take over the main role of interaction. (iii) Finally, for distances and temperatures in the upper-right corner, at $z_a T \gtrsim [(9/2)\sqrt{10}\lambda_\rho/\lambda_{\rm th}]^{1/4}\hbar c/(4\pi k_{\rm B})$, blackbody friction $\mu_T^{\rm vac}$ prevails over the surface contributions. The full line on the left gives the (z_a, T) values for which $\mu_{\rm QF} = \mu_T$, while the full line on the right describes the case where $\mu_T = \mu_T^{\rm vac}$. For our numerical example, we use the critical velocity $v = v_c \equiv \sqrt{2/3}\pi k_{\rm B}T z_a/\hbar$ and once again the parameters given in Fig. 3.

However, for the parameters used in Fig. 5, this never occurs because $T_a < \mathcal{T}_c$.

Figure 6 depicts the ratio $-\mu^r/\mu^t$ as a function of the atom-surface separation and of the temperature for the same parameters of Fig. 3. In general, as for the $T = 0$ case [51], μ^t can be defined starting from Eq. (9) by retaining only the symmetric part of the Green tensor and of the tensor in the curly brackets. Similarly, the expression for the viscosity μ^r can be derived from Eq. (9) by considering the antisymmetric parts of the same tensors. From Eq. (21) we have then that μ^r always identically vanishes if $\mathbf{s}_\perp = 0$. In agreement with our results in Eqs. (26) and (27), we observe a partial cancellation of the two contributions to the viscosity that ranges from 70% to 50%, corresponding to the ratio $-\mu^r/\mu^t$ varying from 5/7 to 1/2. As expected, the crossover between these two values takes place around $z_a/\lambda_c \approx 1$ or $T/T_c \approx 1$.

Finally, Fig. 7 describes the relevance of the different contributions to the electromagnetic viscosity for given velocity in the (z_a, T) plane. While the quantum characteristics of the system ($\mu_{\rm QF}$) are predominant for parameters in the lower-left corner of this plane, the thermal effects start to be more relevant in the remaining part of the plane (μ_T) and eventually recover the case of blackbody friction ($\mu_T^{\rm vac}$) in the upper-right corner.

IV. MATERIAL-MODIFIED SPECTRAL DENSITY

It is also interesting to inspect the behavior of μ_T from another perspective. In the simplest case, where the particle moves through thermal (homogeneous and isotropic) vacuum and no macroscopic bodies are present, we can rewrite Eq. (15) in terms of the thermal part of Planck's blackbody spectrum (the zero-point fluctuations are not relevant for the following considerations) $\varrho(\omega) = \hbar\omega^3 n(\omega)/(\pi^2 c^3)$, i.e.,

$$\mu_T^{\rm vac} \sim -\int_0^\infty d\omega \frac{\omega {\rm Im}[\alpha_{v=0}(\omega)]}{3c^2\epsilon_0} T\,\partial_T\varrho(\omega), \qquad (29)$$

which can be shown to be related to Einstein and Hopf's original result [10,15]. At the given frequency ω, the friction is connected to the slope of the Planck distribution $T\partial_T\varrho(\omega)$ at temperature T, which is accounting for the Doppler shift of the thermal field that the moving atom perceives [15]. The resulting distribution has a maximum and a variance both of the order of the thermal frequency $\omega_{\rm th}$. Importantly, the atom only perceives the part of the spectrum that is within the frequency range of its interaction channels. For instance, if we again consider a single dipole resonance [see Eq. (16) and discussion above], the usually sharp atomic transition acts as a filter, selecting only frequencies $\omega \approx \omega_a$. Mathematically, this is represented in Eq. (29) by the spectral density kernel $\eta^{\rm vac}(\omega) \equiv \omega\,{\rm Im}[\alpha_{v=0}(\omega)]/(3c^2\epsilon_0)$. The interaction is therefore determined by the kind and the strength of the overlap between the spectral density filter and the temperature-dependent behavior of the electromagnetic field. The relation between the maxima and the widths of $\kappa^{\rm vac}(\omega)$ vs $T\partial_T\varrho(\omega)$ determines which of the approximations in Eqs. (16) or (17) is the most adequate.

At low velocities, we can extend this representation to more generic situations and write the thermal viscosity as

$$\mu_T \sim -\int_0^\infty d\omega \eta(\omega) T\,\partial_T\varrho(\omega). \qquad (30)$$

Comparing with the expression in Eq. (13), we can define the spectral density of the joint atom + field system as

$$\eta(\omega) = \frac{2\pi c^3}{\omega^4} \int \frac{dq}{2\pi} \int \frac{d\tilde{q}}{2\pi} q(q-\tilde{q})$$
$$\times \,{\rm Tr}[\underline{\alpha}_{v=0}(\omega)\underline{G}_\Im(\tilde{q}, \mathbf{R}_a, \omega)\underline{\alpha}_{v=0}^\dagger(\omega)\underline{G}_\Im(q, \mathbf{R}_a, \omega)], \qquad (31)$$

which incorporates the interaction with the material-modified electromagnetic field up to all orders in coupling. In this generalization, both the particle's polarizability and the Green tensor of the environment feature characteristic material-dependent resonances that manifest themselves as peaks in the behavior of $\eta(\omega)$, singling out certain frequencies in the interaction with the thermal field. If the temperature is sufficiently high, so that $\omega_{\rm th}$ is larger than the resonances' widths which $T\partial_T\rho(\omega)$ is enclosing, the interaction is resonant and an approximation similar to that in Eq. (16) is possible. Since some of the resonances' widths scale as the inverse of the atom-surface separation, the resonant regime can also take on greater significance for larger distances from the surface. The higher the temperature (or the larger the distance from the surface), though, the more pronounced becomes also the impact of the blackbody radiation $\mu_T^{\rm vac}$ which is independent from the surfaces [see e.g., Eq. (16)]. Conversely, at low temperature, $T\partial_T\rho(\omega)$ is significantly different from zero for ω smaller than all system's resonances, acting as a low-frequency band-pass filter and therefore highlighting the dissipative features of the system. In this case the viscosity given by the integral in Eq. (30) is in the nonresonant regime which we analyzed in Sec. III.

To see this more clearly, let us once again consider the case of a single-resonance polarizability for an atom moving in the near-field of a flat surface. Also, for simplicity, we restrict our discussion to spatially local material models [89]. In Fig. 8 we
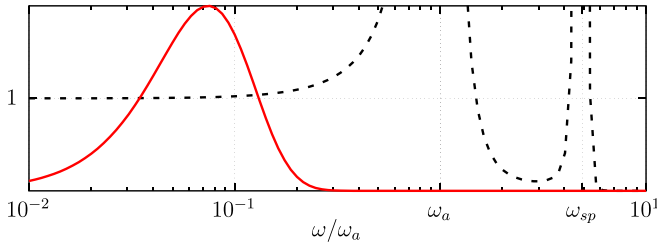
FIG. 8. Scaled representation of the functions composing the integrand in Eq. (30) for the thermal viscosity. Dashed black line: Spectral density of the atom + field system $\eta(\omega)$ [see Eq. (31)] normalized to its low-frequency behavior. We again consider the planar setup in the near field and mark the surface resonance ω_{sp} as well as the single atomic resonance ω_a. Solid red line: $T\partial_T\varrho(\omega)$ evaluated at room temperature divided by half its maximum value. Depending on the chosen value of T, the peak of $T\partial_T\varrho(\omega)$ can accentuate qualitatively different parts of the spectral density [see main text and Eq. (30)]. Setup and parameters are chosen as in Fig. 7 and we use $z_a = 1$ nm.

sketch both the functions in the integrand of Eq. (30) for the case of a ^{87}Rb atom moving above a lead surface (see Fig. 4). For a better visualization, the normalization of each curve is different. The figure highlights that $\eta(\omega)$ contains resonances for $\omega \approx \omega_a$ related to the particle through its polarizability and, if they exist, to the surface ($\omega_{sp} \approx \omega_p/\sqrt{2}$). Examples of the latter are surface-plasmon- and surface-phonon-polariton resonances [47] appearing, respectively, in the case of metallic or dielectric surfaces. Depending on the temperature, the function $T\partial_T\varrho(\omega)$ selects the resonant region of $\eta(\omega)$ or the dissipative low-frequency regime. This gives rise to the resonant or the nonresonant form of frictional interaction, respectively. For comparison, if we take room temperature as a reference, the thermal distribution has a maximum around 5.6% of the value of the resonance frequency of the ^{87}Rb D line [72], substantially overlapping with the low-frequency part of $\eta(\omega)$. For this specific case, one would need a temperature about twenty times larger for the maximum of $T\partial_T\varrho(\omega)$ to reach the value of the atomic transition $\omega_a \approx 1.6$ eV or that of the surface-plasmon resonance $\omega_{sp} \approx 5.2$ eV. The frictional viscosity μ_T would then be characterized by its resonant contribution.

V. CONCLUSION

An atom propelled at constant speed v within a complex electromagnetic environment comprised of several translationally invariant objects at temperature T experiences a force that opposes its motion as if it were moving in a viscous medium. The quantum and thermal fluctuations of the electromagnetic field define a privileged reference frame with respect to which the atom tends to be at rest. In this article, we provide a rather general, self-consistent, nonperturbative and non-Markovian framework which is able to describe many facets of the electromagnetic viscosity felt by the particle. It unifies, completes and extends previous results available in the literature, explaining the processes behind them. Depending on the temperature, the optical response and the geometry of its surroundings as well as the spin angular momentum of the

radiation, the perceived viscosity is characterized by different physical phenomena.

At sufficiently low velocities and temperatures, the frictional interaction is nonresonant and one can distinguish three distinct regimes: (i) At sufficiently large distance z_a from any material interface, the viscosity is dominated by the interaction with the thermal vacuum field. That particular limit recovers what is known in the literature as blackbody friction. Blackbody friction scales linear with the velocity v and the corresponding viscosity depends on the temperature and the parameters characterizing the atom and the electromagnetic radiation in vacuum only. Within this regime we were able to explain why equilibrium-based techniques involving the local thermal equilibrium approximation lead to the correct expression and we identified the limit of this approach. (ii) The closer to an interface the particle moves, the more the interaction is affected by the change in the electromagnetic density of states due to the boundary conditions induced by the material-induced inhomogeneity of space. At sufficiently low velocities, large separation or high temperatures ($k_BT \gg \hbar v/\lambda_a$), the frictional interaction is still mainly thermal. In addition to the parameters determining the drag in vacuum, the viscosity now also depends on the optical properties and the geometry of the objects characterizing the electromagnetic environment as well as on the position of the atom. We have shown in this case that, at the leading order in the velocity, independently from the geometry of the environment and for rather typical material properties, the frictional force scales as $\propto vT^2$ and the corresponding viscosity as $\propto T^2$. Finally, (iii) in the limit of sufficiently low temperatures or comparably short distances or high velocities ($k_BT \ll \hbar v/\lambda_a$), electromagnetic quantum fluctuations become the main source of the interaction, recovering the behavior of quantum friction: Within the nonresonant regime, the quantum drag force is $\propto v^3$, corresponding to a viscosity that scales as v^2. At high temperature or velocities, the frictional interaction becomes resonant and gets enhanced. This regime, however, is not easy to achieve in setups involving atoms and materials typically used in experiments. Our analysis allows us to highlight the characteristic scales and the physical mechanisms which determine the transition between these different regimes. In particular we were able to point out that the quantum properties of the drag force become more relevant for particles with a high kinetic energy. We explained this result by making the connection with the anomalous-Doppler-effect through which virtual excitations (quantum fluctuations) can receive enough energy to turn into real ones at the cost of the atom's kinetic energy.

Similarly to what has already been done for zero temperature [51], our formalism enabled us to identify and characterize a contribution to the frictional processes at finite temperature that involves the exchange of angular momentum between the confined field in the vicinity of the material interface and the particle. We were able to show that, in the nonresonant regime, this contribution, independently from the details of the geometry, diminishes the electromagnetic viscosity. In the specific example of an atom moving at constant velocity in vacuum at nonzero temperature above a planar surface, the transfer of angular momentum turns out to reduce the corresponding viscosity by a factor of one half (at zero temperature the reduction was 5/7).

From the experimental point of view, our results can be of relevance for high-precision experiments with atoms, such as in the design of frequency Refs. [90] or in the interpretation of atom interferometric measurements [91], where blackbody friction, e.g., can be connected to Stark shifts and modified atomic lifetimes [14,92]. Especially with the advent of miniaturization efforts in order to create portable devices of these emerging quantum technologies [93,94], the impact of the instrument's boundaries starts to matter and deviations from the simple Planck spectrum can become important [95,96]. For instance, if we take once again the simplest case of a rubidium atom moving in front of a single lead surface (described via the Drude model) at room temperature, the drag connected to the interaction with the surface starts to exceed the blackbody vacuum drag below separations of some tenths of micrometers. From the perspective of an active detection of the above-discussed effects, we may identify atom interferometry either with cold atoms [91] or in diffraction experiments [97,98] as a promising candidate. The latter is particularly appealing for high velocities (of the order of 1–100 km/s [99]) and small atom-surface separations (a hundred nanometers and thinner) already characterizing recent experiments [100]. The results and the description outlined in the present paper provide the tools that can allow us to better understand and possibly engineer the vacuum viscosity in the presence of (shape-)optimized materials via advanced numerical schemes.

APPENDIX: MATHEMATICAL DETAILS ON THE DERIVATION OF THE FRICTIONAL FORCE

Here we provide additional information about the derivation of some of the expressions presented in the paper.

1. On the expression in Eq. (9)

We start by considering Eq. (9). Following Ref. [47], the Lorentz force acting on the moving dipole can be written as

$$F(t) = \lim_{\mathbf{r} \to \mathbf{r}_a(t)} 2\mathrm{Re}\langle \hat{\mathbf{d}}(t) \cdot \partial_x \hat{\mathbf{E}}^{\oplus}(\mathbf{r}, t)\rangle, \tag{A1}$$

where $\hat{\mathbf{E}}^{\oplus}(\mathbf{r}, t)$ is the part of the total electric-field operator related only to an integration over positive frequencies $\omega \geqslant 0$. As described in Sec. II, the electric-field operator decomposes into two components, i.e., $\hat{\mathbf{E}}(\mathbf{r}, t) = \hat{\mathbf{E}}_0(\mathbf{r}, t) + \hat{\mathbf{E}}_{\mathrm{ind}}(\mathbf{r}, t)$, and each of them can be split in an integration over positive and negative frequencies $\hat{\mathbf{E}}^{\oplus}$ and $\hat{\mathbf{E}}^{\ominus}$, respectively. For $\hat{\mathbf{E}}_0$ we can write

$$\hat{\mathbf{E}}_0^{\oplus}(\mathbf{r}_a(t), t) = \int_0^{\infty} \frac{d\omega}{2\pi} \int \frac{dq}{2\pi} \hat{\mathbf{E}}_0(q, \mathbf{R}_a, \omega) e^{i[qx_a(t) - \omega t]}, \tag{A2}$$

and from Eq. (5) we can obtain the corresponding relation for the field induced by the dipole, $\hat{\mathbf{E}}_{\mathrm{ind}}^{\oplus}(\mathbf{r}, t)$. Accordingly, the force (formally) in Eq. (A1) also decomposes into two parts. In the steady-state ($t \to \infty$), for the contribution to the force connected to $\hat{\mathbf{E}}_0^{\oplus}(\mathbf{r}, t)$, we hence obtain

$$\lim_{\mathbf{r} \to \mathbf{r}_a(t)} 2\mathrm{Re}\langle \hat{\mathbf{d}}(t) \cdot \partial_x \hat{\mathbf{E}}_0^{\oplus}(\mathbf{r}, t)\rangle$$

$$= 2\mathrm{Re} \int \frac{d\tilde{\omega}}{2\pi} \int_0^{\infty} \frac{d\omega}{2\pi} \int \frac{dq}{2\pi} (iq)$$
$$\times \langle \hat{\mathbf{d}}(\tilde{\omega}) \cdot \hat{\mathbf{E}}_0(q, \mathbf{R}_a, \omega)\rangle e^{i[qx_a(t) - (\omega + \tilde{\omega})t]} e^{i\tilde{q}x_0}$$

$$= 2\mathrm{Re} \int \frac{d\tilde{\omega}}{2\pi} \int_0^{\infty} \frac{d\omega}{2\pi} \int \frac{dq}{2\pi} \int \frac{d\tilde{q}}{2\pi} (iq) e^{-i(\omega + \tilde{\omega} - qv)t}$$
$$\times \mathrm{Tr}[\underline{\alpha}_v(\tilde{\omega}) \langle \hat{\mathbf{E}}_0(\tilde{q}, \mathbf{R}_a, \tilde{\omega} + \tilde{q}v) \hat{\mathbf{E}}_0^{\mathsf{T}}(q, \mathbf{R}_a, \omega)\rangle] e^{i(q + \tilde{q})x_0}. \tag{A3}$$

In the previous expression we used that, in the steady-state, the atom's trajectory is given by $x_a(t) \sim x_0 + vt$, where x_0 is the position where system becomes stationary. We also use that the scalar product of two vectors $\mathbf{a}$ and $\mathbf{b}$ is identical to the trace of the dyadic $\mathbf{ab}^{\mathsf{T}}$, i.e., $\mathbf{a} \cdot \mathbf{b} = \mathrm{Tr}[\mathbf{ab}^{\mathsf{T}}]$, and that the steady-state solution for the dynamics of the dipole operator $\hat{\mathbf{d}}(t)$ is given by the stationary solution of Eq. (6). In the frequency domain [see Eq. (7a)] its expression is

$$\hat{\mathbf{d}}(\tilde{\omega}) = \underline{\alpha}_v(\tilde{\omega}) \int \frac{d\tilde{q}}{2\pi} \hat{\mathbf{E}}_0(\tilde{q}, \mathbf{R}_a, \tilde{\omega} + \tilde{q}v) e^{i\tilde{q}x_0}. \tag{A4}$$

Since $\hat{\mathbf{E}}_0$ describes the field without the atom, the dyadic $\langle \hat{\mathbf{E}}_0(\tilde{q}, \mathbf{R}_a, \tilde{\omega} + \tilde{q}v) \hat{\mathbf{E}}_0^{\mathsf{T}}(q, \mathbf{R}_a, \omega)\rangle$ can be evaluated using the fluctuation-dissipation relation in Eq. (3). Finally, we obtain

$$\lim_{\mathbf{r} \to \mathbf{r}_a(t)} 2\mathrm{Re}\langle \hat{\mathbf{d}}(t) \cdot \partial_x \hat{\mathbf{E}}_0^{\oplus}(\mathbf{r}, t)\rangle$$

$$= 4\hbar \mathrm{Re} \int_0^{\infty} \frac{d\omega}{2\pi} \int \frac{dq}{2\pi} iqn(\omega) \mathrm{Tr}[\underline{\alpha}_v(-\omega_q^-) \underline{G}_{\Im}^{\mathsf{T}}(q, \mathbf{R}_a, \omega)], \tag{A5}$$

where we used that $-\underline{G}_{\Im}^{\mathsf{T}}(q, \mathbf{R}_a, \omega) = \underline{G}_{\Im}(-q, \mathbf{R}_a, -\omega)$, $n(-\omega) = -[1 + n(\omega)]$. If we now evaluate the real part of the expression, we arrive at

$$\lim_{\mathbf{r} \to \mathbf{r}_a(t)} 2\mathrm{Re}\langle \hat{\mathbf{d}}(t) \cdot \partial_x \hat{\mathbf{E}}_0^{\oplus}(\mathbf{r}, t)\rangle$$

$$= -4\hbar \int_0^{\infty} \frac{d\omega}{2\pi} \int \frac{dq}{2\pi} qn(\omega)$$
$$\times \mathrm{Tr}\left[\frac{\underline{\alpha}_v(-\omega_q^-) \underline{G}_{\Im}^{\mathsf{T}}(q, \mathbf{R}_a, \omega) - \underline{\alpha}_v^*(-\omega_q^-) \underline{G}_{\Im}^{\dagger}(q, \mathbf{R}_a, \omega)}{2i}\right]$$

$$= -2\frac{\hbar}{\pi} \int_0^{\infty} d\omega \int \frac{dq}{2\pi} qn(\omega) \mathrm{Tr}[\underline{\alpha}_{v,\Im}(-\omega_q^-) \underline{G}_{\Im}^{\mathsf{T}}(q, \mathbf{R}_a, \omega)], \tag{A6}$$

where we used in the second line that $\underline{G}_{\Im}(q, \mathbf{R}_a, \omega) = \underline{G}_{\Im}^{\dagger}(q, \mathbf{R}_a, \omega)$ and that the trace of a matrix is identical to the trace of its transpose. The previous result gives the first term on the r.h.s of Eq. (9). The second term on the r.h.s of Eq. (9) has been derived in earlier work [47]. Combining the two, we arrive at Eq. (9).

2. On the expression in Eq. (10)

Let us now derive the equivalent expression for the frictional interaction presented in Eq. (10). Starting from Eq. (9), we first substitute $\omega \to \omega + qv = \omega_q^+$, i.e.,

$$F = -2 \int \frac{dq}{2\pi} \int_{-qv}^{\infty} d\omega\, q\, \mathrm{Tr}\bigg[\bigg\{\frac{\hbar}{\pi} n(\omega_q^+) \underline{\alpha}_{v,\Im}(-\omega)$$
$$+ \underline{S}_v(-\omega)\bigg\} \underline{G}_\Im^\mathsf{T}(q, \mathbf{R}_a, \omega_q^+)\bigg]. \tag{A7}$$

Second, we employ the identities $\underline{\alpha}_{v,\Im}(-\omega) = -\underline{\alpha}_{v,\Im}^\mathsf{T}(\omega)$ and $\underline{S}_v(-\omega) = \underline{S}_v^\mathsf{T}(\omega) - (\hbar/\pi)\underline{\alpha}_\Im^\mathsf{T}(\omega)$ to obtain

$$F = 2 \int \frac{dq}{2\pi} \int_{-qv}^{\infty} d\omega\, q\, \mathrm{Tr}\bigg[\bigg\{\frac{\hbar}{\pi}[1 + n(\omega_q^+)]\underline{\alpha}_{v,\Im}^\mathsf{T}(\omega)$$
$$- \underline{S}_v^\mathsf{T}(\omega)\bigg\} \underline{G}_\Im^\mathsf{T}(q, \mathbf{R}_a, \omega_q^+)\bigg]. \tag{A8}$$

The properties of the trace operation allow us to remove the "T" superscript in the previous expression. The only difference with respect to Eq. (10) is that the integral over the frequencies runs from $-qv$ instead of zero. Interestingly, however, upon substituting $\omega \to -\omega$ and $q \to -q$, we have that

$$\int \frac{dq}{2\pi} \int_{-qv}^{0} d\omega\, q\, \mathrm{Tr}\bigg[\bigg\{\frac{\hbar}{\pi}[1 + n(\omega_q^+)]\underline{\alpha}_{v,\Im}(\omega)$$
$$- \underline{S}_v(\omega)\bigg\} \underline{G}_\Im(q, \mathbf{R}_a, \omega_q^+)\bigg]$$
$$= \int \frac{dq}{2\pi} \int_{-qv}^{0} d\omega\, q\, \mathrm{Tr}\bigg[\bigg\{\frac{\hbar}{\pi} n(\omega_q^+)\underline{\alpha}_{v,\Im}(-\omega)$$
$$+ \underline{S}_v(-\omega)\bigg\} \underline{G}_\Im^\mathsf{T}(q, \mathbf{R}_a, \omega_q^+)\bigg]$$
$$= -\int \frac{dq}{2\pi} \int_{-qv}^{0} d\omega\, q\, \mathrm{Tr}\bigg[\bigg\{\frac{\hbar}{\pi}[1 + n(\omega_q^+)]\underline{\alpha}_{v,\Im}(\omega)$$
$$- \underline{S}_v(\omega)\bigg\} \underline{G}_\Im(q, \mathbf{R}_a, \omega_q^+)\bigg]. \tag{A9}$$

Here, we used again the identities for the polarizability and the power spectrum given after Eq. (A7) as well as those for the Bose number and the Green tensor given after Eq. (10). The above result indicates that this contribution is zero and that we can replace the frequency integration range in Eq. (A8) from $[-qv, \infty)$ to $[0, \infty)$, recovering Eq. (10).

3. On the expression in Eq. (11)

It is also interesting to show that the previous results can be obtained using the symmetric ordering of operators instead of the ordering used in the main text. Our starting point is the Lorentz force given by Eq. (4) of the main text, written in the symmetrized form

$$F(t) = \lim_{\mathbf{r} \to \mathbf{r}_a} \langle \hat{\mathbf{d}}(t) \cdot \partial_x \hat{\mathbf{E}}(\mathbf{r}, t)\rangle_{\mathrm{sym}}, \tag{A10}$$

where the symmetric average is defined as

$$\langle \hat{\mathbf{A}} \cdot \hat{\mathbf{B}}\rangle_{\mathrm{sym}} \equiv \frac{\langle \hat{\mathbf{A}} \cdot \hat{\mathbf{B}} + \hat{\mathbf{B}} \cdot \hat{\mathbf{A}}\rangle}{2} = \frac{\langle \hat{A}_i \hat{B}_i + \hat{B}_i \hat{A}_i\rangle}{2} \tag{A11}$$

(in the last line we implicitly summed over the repeated indices). While the operator ordering is irrelevant in Eq. (A10), this is no longer true if we consider again the splitting $\hat{\mathbf{E}}(\mathbf{r}, t) = \hat{\mathbf{E}}_0(\mathbf{r}, t) + \hat{\mathbf{E}}_{\mathrm{ind}}(\mathbf{r}, t)$ and calculated the corresponding terms independently.

We start with the contribution to the force connected to the vacuum part of the field operator $\hat{\mathbf{E}}_0$ and obtain at late times

$$\lim_{\mathbf{r} \to \mathbf{r}_a(t)} \langle \hat{\mathbf{d}}(t) \cdot \partial_x \hat{\mathbf{E}}_0(\mathbf{r}, t)\rangle_{\mathrm{sym}}$$
$$= \lim_{\mathbf{r} \to \mathbf{r}_a} \int \frac{d\omega}{2\pi} e^{-i\omega t} \langle \hat{\mathbf{d}}(\omega) \cdot \partial_x \hat{\mathbf{E}}_0(\mathbf{r}, t)\rangle_{\mathrm{sym}}$$
$$= \int \frac{d\omega}{2\pi} \int \frac{d\tilde{\omega}}{2\pi} \int \frac{d\tilde{q}}{2\pi} (i\tilde{q}) e^{-i\omega t} e^{i[\tilde{q}x_a(t) - \tilde{\omega}t]}$$
$$\times \langle \hat{\mathbf{d}}(\omega) \cdot \hat{\mathbf{E}}_0(\tilde{q}, \mathbf{R}_a, \tilde{\omega})\rangle_{\mathrm{sym}}$$
$$= \int \frac{d\omega}{2\pi} \int \frac{d\tilde{\omega}}{2\pi} \int \frac{d\tilde{q}}{2\pi} \int \frac{dq}{2\pi} e^{i(\tilde{q}v - \tilde{\omega} - \omega)t} e^{i(q + \tilde{q})x_0}$$
$$\times (i\tilde{q}) \mathrm{Tr}[\underline{\alpha}_v(\omega) \langle \hat{\mathbf{E}}_0(q, \mathbf{R}_a, \omega + qv) \hat{\mathbf{E}}_0^\mathsf{T}(\tilde{q}, \mathbf{R}_a, \tilde{\omega})\rangle_{\mathrm{sym}}]. \tag{A12}$$

In the case of the dyadic product of vector operators, the symmetric average has to be understood componentwise, i.e., $[\langle \hat{\mathbf{A}}\hat{\mathbf{B}}^\mathsf{T}\rangle_{\mathrm{sym}}]_{ij} = \langle A_i B_j + B_j A_i\rangle/2$. In terms of the matrices resulting from the dyadic product, this can be written as $\langle \hat{\mathbf{A}}\hat{\mathbf{B}}^\mathsf{T}\rangle_{\mathrm{sym}} = \langle \hat{\mathbf{A}}\hat{\mathbf{B}}^\mathsf{T}\rangle + \langle \hat{\mathbf{B}}\hat{\mathbf{A}}^\mathsf{T}\rangle^\mathsf{T}/2$. The symmetric average of the vacuum field can be computed by replacing $2[1 + n(\omega)] \to \coth[\hbar\omega/(2k_BT)]$ in Eq. (3). This yields

$$\lim_{\mathbf{r} \to \mathbf{r}_a(t)} \langle \hat{\mathbf{d}}(t) \cdot \partial_x \hat{\mathbf{E}}_0(\mathbf{r}, t)\rangle_{\mathrm{sym}}$$
$$= -\hbar \int \frac{d\omega}{2\pi} \int \frac{dq}{2\pi} (iq) \coth\left(\frac{\hbar\omega_q^+}{2k_BT}\right)$$
$$\times \mathrm{Tr}[\underline{\alpha}_v(\omega) \underline{G}_\Im(q, \mathbf{R}_a, \omega_q^+)]$$
$$= -\hbar \int_0^\infty \frac{d\omega}{2\pi} \int \frac{dq}{2\pi} (iq) \coth\left(\frac{\hbar\omega_q^+}{2k_BT}\right)$$
$$\times \{\mathrm{Tr}[\underline{\alpha}_v(\omega) - \underline{\alpha}_v^\dagger(\omega)\} \underline{G}_\Im(q, \mathbf{R}_a, \omega_q^+)]$$
$$= \frac{\hbar}{\pi} \int_0^\infty d\omega \int \frac{dq}{2\pi} q \coth\left(\frac{\hbar\omega_q^+}{2k_BT}\right)$$
$$\times \mathrm{Tr}[\underline{\alpha}_{v,\Im}(\omega) \underline{G}_\Im(q, \mathbf{R}_a, \omega_q^+)]. \tag{A13}$$

For the part of the force connected to $\hat{\mathbf{E}}_{\mathrm{ind}}$, we employ Eq. (5) and use that at late times we can write

$$\hat{\mathbf{E}}_{\mathrm{ind}}(\mathbf{r}, t) = \int_{-\infty}^{t-t_0} d\tau\, \underline{G}(\mathbf{r}(t), \mathbf{r}_a(t - \tau), \tau) \hat{\mathbf{d}}(t - \tau)$$
$$\stackrel{t, -t_0 \to \infty}{=} \int d\tau \int \frac{d\omega}{2\pi} \int \frac{d\omega'}{2\pi} \int \frac{dq}{2\pi} \underline{G}(q, \mathbf{R}_a, \tilde{\omega}) \hat{\mathbf{d}}(\omega)$$
$$\times e^{-i(\tilde{\omega} - \omega)\tau - i\omega t} e^{iq[x - x_a(t - \tau)]}, \tag{A14}$$

where we could extend the convolution in the first line to $\tau \to -\infty$ since the Green tensor is a causal function. Upon inserting the expression for the steady-state atom's trajectory $x_a(t) \sim x_0 + vt$ into the symmetrized expression of the force,

we obtain

$$\lim_{\mathbf{r}\to\mathbf{r}_a(t)}\langle \hat{\mathbf{d}}(t)\cdot\partial_x\hat{\mathbf{E}}_{\mathrm{ind}}(\mathbf{r},t)\rangle_{\mathrm{sym}} \sim \int d\tau \int\frac{d\omega}{2\pi}\int\frac{d\tilde\omega}{2\pi}\int\frac{d\nu}{2\pi}\int\frac{dq}{2\pi}(iq)\langle\hat{\mathbf{d}}(\nu)\cdot\underline{G}(q,\mathbf{R}_a,\tilde\omega)\hat{\mathbf{d}}(\omega)\rangle_{\mathrm{sym}}e^{-i(\tilde\omega-\omega-qv)\tau-i(\omega+\nu)t}$$

$$=\hbar\int\frac{d\omega}{2\pi}\int\frac{dq}{2\pi}\int\frac{d\tilde q}{2\pi}(iq)\coth\left(\frac{\hbar\omega_{\tilde q}^+}{2k_{\mathrm B}T}\right)\mathrm{Tr}[\underline{\alpha}_v(\omega)\underline{G}_\Im(\tilde q,\mathbf{R}_a,\omega_{\tilde q}^+)\underline{\alpha}_v^\dagger(\omega)\underline{G}(q,\mathbf{R}_a,\omega_q^+)]$$

$$=\hbar\int_0^\infty\frac{d\omega}{2\pi}\int\frac{dq}{2\pi}\int\frac{d\tilde q}{2\pi}(iq)\coth\left(\frac{\hbar\omega_{\tilde q}^+}{2k_{\mathrm B}T}\right)\{\mathrm{Tr}[\underline{\alpha}_v(\omega)\underline{G}_\Im(\tilde q,\mathbf{R}_a,\omega_{\tilde q}^+)\underline{\alpha}_v^\dagger(\omega)\underline{G}(q,\mathbf{R}_a,\omega_q^+)]$$

$$-\ \mathrm{Tr}[\underline{\alpha}_v^*(\omega)\underline{G}_\Im^\mathsf{T}(\tilde q,\mathbf{R}_a,\omega_{\tilde q}^+)\underline{\alpha}_v^\mathsf{T}(\omega)\underline{G}^*(q,\mathbf{R}_a,\omega_q^+)]\}$$

$$=-\frac{\hbar}{\pi}\int_0^\infty d\omega\int\frac{dq}{2\pi}\int\frac{d\tilde q}{2\pi}q\coth\left(\frac{\hbar\omega_{\tilde q}^+}{2k_{\mathrm B}T}\right)\mathrm{Tr}[\underline{\alpha}_v(\omega)\underline{G}_\Im(\tilde q,\mathbf{R}_a,\omega_{\tilde q}^+)\underline{\alpha}_v^\dagger(\omega)\underline{G}_\Im(q,\mathbf{R}_a,\omega_q^+)], \tag{A15}$$

where, together with the properties of the trace operation, we used that $\underline{G}(-q,\mathbf{R}_a,-\omega)=\underline{G}^*(q,\mathbf{R}_a,\omega)$ and that, similarly to the electromagnetic field, the symmetric dipole correlator can be obtained by replacing in Eq. (7) $n(\omega_q^+)+1\to$ $\coth[\hbar\omega_q^+/(2k_{\mathrm B}T)]/2$. Adding Eqs. (A13) and (A15) we arrive at Eq. (11), which is equivalent to the expressions in Eqs. (9) and (10) obtained using a different approach and ordering scheme.

---

[1] E. Noether, Invariante Variationsprobleme, Nachrichten von der Gesellschaft der Wissenschaften zu Göttingen, Mathematisch-Physikalische Klasse **1918**, 235 (1918).

[2] S. A. Fulling and P. C. W. Davies, Radiation from a moving mirror in two dimensional space-time: Conformal anomaly, Proc. R. Soc. London, Ser. A **348**, 393 (1976).

[3] P. C. W. Davies, Scalar production in schwarzschild and rindler metrics, J. Phys. A: Math. Gen. **8**, 609 (1975).

[4] B. S. DeWitt, Quantum field theory in curved spacetime, Phys. Rep. **19**, 295 (1975).

[5] W. G. Unruh, Notes on black-hole evaporation, Phys. Rev. D: Part. Fields **14**, 870 (1976).

[6] D. A. R. Dalvit and P. A. Maia Neto, Decoherence via the Dynamical Casimir Effect, Phys. Rev. Lett. **84**, 798 (2000).

[7] V. Dodonov, Fifty years of the dynamical Casimir effect, Physics (Basel) **2**, 67 (2009).

[8] M.-T. Jaekel and S. Reynaud, Friction and inertia for a mirror in a thermal field, Phys. Lett. A **172**, 319 (1993).

[9] L. A. S. Machado, P. A. Maia Neto, and C. Farina, Quantum radiation pressure on a moving mirror at finite temperature, Phys. Rev. D: Part. Fields **66**, 105016 (2002).

[10] A. Einstein and L. Hopf, Statistische untersuchung der bewegung eines resonators in einem strahlungsfeld, Ann. Phys. (Berlin, Ger.) **338**, 1105 (1910).

[11] P. W. Milonni, Quantum mechanics of the Einstein–Hopf model, Am. J. Phys. **49**, 177 (1981).

[12] G. W. Ford, J. T. Lewis, and R. F. O'Connell, Quantum Oscillator in a Blackbody Radiation Field, Phys. Rev. Lett. **55**, 2273 (1985).

[13] V. Mkrtchian, V. Parsegian, R. Podgornik, and W. Saslow, Universal Thermal Radiation Drag on Neutral Objects, Phys. Rev. Lett. **91**, 220801 (2003).

[14] G. Łach, M. DeKieviet, and U. D. Jentschura, Enhancement of Blackbody Friction due to the Finite Lifetime of Atomic Levels, Phys. Rev. Lett. **108**, 043005 (2012).

[15] G. Łach, M. DeKieviet, and U. Jentschura, Einstein-Hopf drag, Doppler shift of thermal radiation and blackbody drag: Three perspectives on quantum friction, Open Physics **10**, 763 (2012).

[16] U. D. Jentschura, G. Łach, M. De Kieviet, and K. Pachucki, One-Loop Dominance in the Imaginary Part of the Polarizability: Application to Blackbody and Noncontact van der Waals Friction, Phys. Rev. Lett. **114**, 043001 (2015).

[17] G. V. Dedkov and A. A. Kyasov, Radiation of a neutral polarizable particle moving uniformly through a thermal radiation field, Phys. Scr. **89**, 105501 (2014).

[18] A. I. Volokitin, Friction force at the motion of a small relativistic neutral particle with respect to blackbody radiation, JETP Lett. **101**, 427 (2015).

[19] P. A. Maia Neto and C. Farina, Comment on "Universal Thermal Radiation Drag on Neutral Objects," Phys. Rev. Lett. **93**, 059001 (2004).

[20] S. Kaur, B. Arora, and B. K. Sahoo, Roles of Blackbody Friction Forces in the Rb and Cs Atom Interferometers, arXiv:2012.07362.

[21] G. V. Dedkov and A. A. Kyasov, Fluctuation-electromagnetic interaction under dynamic and thermal nonequilibrium conditions, Phys. Usp. **60**, 559 (2017).

[22] D. Reiche, F. Intravaia, and K. Busch, Wading through the void: Exploring quantum friction and nonequilibrium fluctuations, APL Photonics **7**, 030902 (2022).

[23] For practical reasons, the units of μ do not identically coincide with its classical counterpart.

[24] A. Nourtier, Friction coefficient of atoms near a metal surface, J. Phys. (Paris) **38**, 479 (1977).

[25] M. S. Tomassone and A. Widom, Electronic friction forces on molecules moving near metals, Phys. Rev. B **56**, 4938 (1997).

[26] J. B. Pendry, Shearing the vacuum - quantum friction, J. Phys.: Condens. Matter **9**, 10301 (1997).

[27] J. R. Zurita-Sánchez, J.-J. Greffet, and L. Novotny, Friction forces arising from fluctuating thermal fields, Phys. Rev. A **69**, 022902 (2004).

[28] J. S. Høye, I. Brevik, and K. A. Milton, Casimir friction between polarizable particle and half-space with radiation

damping at zero temperature, J. Phys. A: Math. Theor. **48**, 365004 (2015).

[29] A. I. Volokitin and B. N. J. Persson, Near-field radiative heat transfer and noncontact friction, Rev. Mod. Phys. **79**, 1291 (2007).

[30] S. Scheel and S. Y. Buhmann, Casimir-Polder forces on moving atoms, Phys. Rev. A **80**, 042902 (2009).

[31] F. Intravaia, C. Henkel, and M. Antezza, in *Casimir Physics*, Vol. 834 of *Lecture Notes in Physics*, edited by D. Dalvit, P. Milonni, D. Roberts, and F. da Rosa (Springer, Berlin, Heidelberg, 2011), pp. 345–391.

[32] G. Pieplow and C. Henkel, Fully covariant radiation force on a polarizable particle, New J. Phys. **15**, 023027 (2013).

[33] V. A. Golyk, M. Krüger, and M. Kardar, Linear response relations in fluctuational electrodynamics, Phys. Rev. B **88**, 155117 (2013).

[34] A. Manjavacas, F. J. Rodríguez-Fortuño, F. J. García de Abajo, and A. V. Zayats, Lateral Casimir Force on a Rotating Particle near a Planar Surface, Phys. Rev. Lett. **118**, 133605 (2017).

[35] M. B. Farias, C. D. Fosco, F. C. Lombardo, and F. D. Mazzitelli, Quantum friction between graphene sheets, Phys. Rev. D **95**, 065012 (2017).

[36] M. B. Farías, C. D. Fosco, F. C. Lombardo, and F. D. Mazzitelli, Motion induced radiation and quantum friction for a moving atom, Phys. Rev. D **100**, 036013 (2019).

[37] S. Sanders, W. J. M. Kort-Kamp, D. A. R. Dalvit, and A. Manjavacas, Nanoscale transfer of angular momentum mediated by the Casimir torque, Commun. Phys. **2**, 71 (2019).

[38] D. Pan, H. Xu, and F. J. García de Abajo, Magnetically activated rotational vacuum friction, Phys. Rev. A **99**, 062509 (2019).

[39] M. Lee, R. L. C. Vink, C. A. Volkert, and M. Krüger, Noncontact friction: Role of phonon damping and its nonuniversality, Phys. Rev. B **104**, 174309 (2021).

[40] L. Viotti, M. Belén Farías, P. I. Villar, and F. C. Lombardo, Thermal corrections to quantum friction and decoherence: A closed-time-path approach to atom-surface interaction, Phys. Rev. D **99**, 105005 (2019).

[41] X. Guo, K. A. Milton, G. Kennedy, W. P. McNulty, N. Pourtolami, and Y. Li, Energetics of quantum vacuum friction: Field fluctuations, Phys. Rev. D **104**, 116006 (2021).

[42] J.-T. Hsiang and B.-L. Hu, Nonequilibrium quantum free energy and effective temperature, generating functional, and influence action, Phys. Rev. D **103**, 065001 (2021).

[43] A. I. Volokitin and B. N. Y. Persson, Quantum Cherenkov radiation at the motion of a small neutral particle parallel to the surface of a transparent dielectric, JETP Lett. **103**, 228 (2016).

[44] F. Intravaia, Vacuum Incalescence, arXiv:1604.02990.

[45] D. Reiche, Ph.D. thesis, Long-time correlations in nonequilibrium dispersion forces, University library of the Humboldt-Universität zu Berlin, 2021, doi: 10.18452/22412.

[46] F. Intravaia, R. O. Behunin, C. Henkel, K. Busch, and D. A. R. Dalvit, Failure of Local Thermal Equilibrium in Quantum Friction, Phys. Rev. Lett. **117**, 100402 (2016).

[47] F. Intravaia, R. O. Behunin, C. Henkel, K. Busch, and D. A. R. Dalvit, Non-Markovianity in atom-surface dispersion forces, Phys. Rev. A **94**, 042114 (2016).

[48] D. Reiche, F. Intravaia, J.-T. Hsiang, K. Busch, and B. L. Hu, Nonequilibrium thermodynamics of quantum friction, Phys. Rev. A **102**, 050203(R) (2020).

[49] Y. Oi Nakamura, Spin quantum number of surface plasmon, Solid State Commun. **39**, 763 (1981).

[50] K. Y. Bliokh, D. Smirnova, and F. Nori, Quantum spin Hall effect of light, Science **348**, 1448 (2015).

[51] F. Intravaia, M. Oelschläger, D. Reiche, D. A. R. Dalvit, and K. Busch, Quantum Rolling Friction, Phys. Rev. Lett. **123**, 120401 (2019).

[52] The code package "QuaCa" used to perform the numerical computations can be found at https://github.com/QuaCaTeam/quaca.git.

[53] D. Reiche, K. Busch, and F. Intravaia, Nonadditive Enhancement of Nonequilibrium Atom-Surface Interactions, Phys. Rev. Lett. **124**, 193603 (2020).

[54] E. Vetsch, D. Reitz, G. Sagué, R. Schmidt, S. T. Dawkins, and A. Rauschenbeutel, Optical Interface Created by Laser-Cooled Atoms Trapped in the Evanescent Field Surrounding an Optical Nanofiber, Phys. Rev. Lett. **104**, 203603 (2010).

[55] O. A. Schmidt, T. G. Euser, and P. S. Russell, Mode-based microparticle conveyor belt in air-filled hollow-core photonic crystal fiber, Opt. Express **21**, 29383 (2013).

[56] R. Kubo, The fluctuation-dissipation theorem, Rep. Prog. Phys. **29**, 255 (1966).

[57] M. R. Dennis, Geometric interpretation of the three-dimensional coherence matrix for nonparaxial polarization, J. Opt. A **6**, S26 (2004).

[58] K. Y. Bliokh, F. J. Rodríguez-Fortuño, F. Nori, and A. V. Zayats, Spin–orbit interactions of light, Nat. Photonics **9**, 796 (2015).

[59] F. Intravaia, R. O. Behunin, and D. A. R. Dalvit, Quantum friction and fluctuation theorems, Phys. Rev. A **89**, 050101(R) (2014).

[60] B. Hu, J. Paz, and Y. Zhang, Quantum Brownian motion in a general environment: Exact master equation with nonlocal dissipation and colored noise, Phys. Rev. D: Part. Fields **45**, 2843 (1992).

[61] F. Intravaia and R. Behunin, Casimir effect as a sum over modes in dissipative systems, Phys. Rev. A **86**, 062517 (2012).

[62] P. W. Milonni, J. R. Ackerhalt, and W. A. Smith, Interpretation of Radiative Corrections in Spontaneous Emission, Phys. Rev. Lett. **31**, 958 (1973).

[63] J. Dalibard, J. Dupont-Roc, and C. Cohen-Tannoudji, Vacuum fluctuations and radiation reaction: Identification of their respective contributions, J. Phys. (Paris) **43**, 1617 (1982).

[64] J. Durnin, J. Klatt, R. Bennett, and S. Y. Buhmann, Spectroscopic effects of velocity-dependent Casimir-Polder interactions induced by parallel plates, Phys. Rev. A **105**, 032822 (2022).

[65] F. Intravaia, V. E. Mkrtchian, S. Y. Buhmann, S. Scheel, D. A. R. Dalvit, and C. Henkel, Friction forces on atoms after acceleration, J. Phys.: Condens. Matter **27**, 214020 (2015).

[66] K. Joulain, R. Carminati, J.-P. Mulet, and J.-J. Greffet, Definition and measurement of the local density of electromagnetic states close to an interface, Phys. Rev. B **68**, 245405 (2003).

[67] P. Lodahl, S. Mahmoodian, S. Stobbe, A. Rauschenbeutel, P. Schneeweiss, J. Volz, H. Pichler, and P. Zoller, Chiral quantum optics, Nature (London) **541**, 473 EP (2017).

[68] M. S. Tomaš, Green function for multilayers: Light scattering in planar cavities, Phys. Rev. A **51**, 2545 (1995).

[69] C. Tai, I. Antennas, P. Society, I. M. Theory, and T. Society, *Dyadic Green Functions in Electromagnetic Theory*, *IEEE*

Press Series on Electromagnetic Waves (IEEE Press, New York, 1994).

[70] J. D. Jackson, *Classical Electrodynamics*, 3rd ed. (Wiley, New York, 1999).

[71] M. Oelschläger, K. Busch, and F. Intravaia, Nonequilibrium atom-surface interaction with lossy multilayer structures, Phys. Rev. A **97**, 062507 (2018).

[72] D. A. Steck, Technical report, Oregon Center for Optics and Department of Physics, University of Oregon (unpublished), http://steck.us/alkalidata/.

[73] Some dielectrics, such as silicon nitride or glass, feature polaritonic resonances which can be comparable to thermal energies for temperatures T usually higher than room temperature but still reachable in experiments (e.g., the SiC-vacuum interface features a surface resonance around 120 meV [101]). This was, for example, used in the context of radiative heat transfer [102,103]. For comparison, for metals surface plasmon-polariton frequencies are typically around a few eV [104].

[74] R. Estrada and R. P. Kanwal, *Asymptotic Analysis: A Distributional Approach* (Birkhäuser Boston, Boston, 1994).

[75] R. Estrada and S. A. Fulling, How singular functions define distributions, J. Phys. A: Math. Gen. **35**, 3079 (2002).

[76] G. V. Dedkov and A. A. Kyasov, Electromagnetic and fluctuation-electromagnetic forces of interaction of moving particles and nanoprobes with surfaces: A nonrelativistic consideration, Phys. Solid State **44**, 1809 (2002).

[77] K. A. Milton, J. S. Høye, and I. Brevik, The reality of Casimir friction, Symmetry **8**, 29 (2016).

[78] J. Klatt, C. M. Kropf, and S. Y. Buhmann, Open Quantum Systems' Decay across Time, Phys. Rev. Lett. **126**, 210401 (2021).

[79] A. I. Volokitin and B. N. J. Persson, Dissipative van der Waals interaction between a small particle and a metal surface, Phys. Rev. B **65**, 115419 (2002).

[80] Physically, $\underline{G}_{\Im}(q, \mathbf{R}_a, \omega)$ must be positive semidefinite (for $\omega > 0$) since it is connected with the power emitted by a point-like dipole in a complex medium with only passive materials. Given that $\underline{G}_{\Im}(q, \mathbf{R}_a, 0) = 0$, we can also conclude that $\underline{G}'_{\Im}(\tilde{q}, \mathbf{R}_a, 0) = \lim_{\omega \to 0^+} \underline{G}_{\Im}(q, \mathbf{R}_a, \omega)/\omega > 0$. Also, in the decomposition involving the matrix $\underline{\Sigma}$ and the real vector $\mathbf{s}_\perp$, $\underline{\Sigma}$ is positive semidefinite since it is the symmetric part of $\underline{G}_{\Im}$ and therefore the sum of two positive semidefinite matrices.

[81] V. L. Ginzburg, Certain theoretical aspects of radiation due to superluminal motion in a medium, Sov. Phys. Usp. **2**, 874 (1960).

[82] M. V. Nezlin, Negative-energy waves and the anomalous Doppler effect, Sov. Phys. Usp. **19**, 946 (1976).

[83] M. F. Maghrebi, R. Golestanian, and M. Kardar, Quantum Cherenkov radiation and noncontact friction, Phys. Rev. A **88**, 042509 (2013).

[84] A. Volokitin and B. Persson, Quantum field theory of van der Waals friction, Phys. Rev. B **74**, 205413 (2006).

[85] U. D. Jentschura, M. Janke, and M. DeKieviet, Theory of noncontact friction for atom-surface interactions, Phys. Rev. A **94**, 022510 (2016).

[86] G. Pieplow and C. Henkel, Cherenkov friction on a neutral particle moving parallel to a dielectric, J. Phys.: Condens. Matter **27**, 214001 (2015).

[87] M. A. Ordal, L. L. Long, R. J. Bell, S. E. Bell, R. R. Bell, R. W. Alexander, and C. A. Ward, Optical properties of the metals Al, Co, Cu, Au, Fe, Pb, Ni, Pd, Pt, Ag, Ti, and W in the infrared and far infrared, Appl. Opt. **22**, 1099 (1983).

[88] M. A. Ordal, R. J. Bell, R. W. Alexander, L. L. Long, and M. R. Querry, Optical properties of fourteen metals in the infrared and far infrared: Al, Co, Cu, Au, Fe, Pb, Mo, Ni, Pd, Pt, Ag, Ti, V, and W, Appl. Opt. **24**, 4493 (1985).

[89] D. Reiche, D. A. R. Dalvit, K. Busch, and F. Intravaia, Spatial dispersion in atom-surface quantum friction, Phys. Rev. B **95**, 155448 (2017).

[90] A. D. Ludlow, M. M. Boyd, J. Ye, E. Peik, and P. O. Schmidt, Optical atomic clocks, Rev. Mod. Phys. **87**, 637 (2015).

[91] S. Abend *et al.*, in *Volume 197: Foundations of Quantum Theory*, Vol. 834 of *Proceedings of the International School of Physics "Enrico Fermi,"* edited by E. M. Rasel, W. P. Schleich, and S. Wölk (IOS Press Ebooks, Amsterdam, 2019), pp. 345–392.

[92] J. W. Farley and W. H. Wing, Accurate calculation of dynamic Stark shifts and depopulation rates of Rydberg energy levels induced by blackbody radiation. hydrogen, helium, and alkali-metal atoms, Phys. Rev. A **23**, 2397 (1981).

[93] T. Schuldt *et al.*, Optical clock technologies for global navigation satellite systems, GPS Solut. **25**, 83 (2021).

[94] K. Bongs *et al.*, Taking atom interferometric quantum sensors from the laboratory to real-world applications, Nat. Rev. Phys. **1**, 731 (2019).

[95] B. E. Kalensher, Blackbody radiation from cubes and spheres with application to rapid solidification of microspheres, J. Appl. Phys. **56**, 1347 (1984).

[96] A. M. García-García, Finite-size corrections to the blackbody radiation laws, Phys. Rev. A **78**, 023806 (2008).

[97] A. D. Cronin, J. Schmiedmayer, and D. E. Pritchard, Optics and interferometry with atoms and molecules, Rev. Mod. Phys. **81**, 1051 (2009).

[98] K. Hornberger, S. Gerlich, P. Haslinger, S. Nimmrichter, and M. Arndt, Colloquium: quantum interference of clusters and molecules, Rev. Mod. Phys. **84**, 157 (2012).

[99] C. Brand, M. Debiossac, T. Susi, F. Aguillon, J. Kotakoski, P. Roncin, and M. Arndt, Coherent diffraction of hydrogen through the 246 pm lattice of graphene, New J. Phys. **21**, 033004 (2019).

[100] J. D. Perreault and A. D. Cronin, Observation of Atom Wave Phase Shifts Induced by Van Der Waals Atom-Surface Interactions, Phys. Rev. Lett. **95**, 133201 (2005).

[101] K. Joulain, J.-P. Mulet, F. Marquier, R. Carminati, and J.-J. Greffet, Surface electromagnetic waves thermally excited: Radiative heat transfer, coherence properties and Casimir forces revisited in the near field, Surf. Sci. Rep. **57**, 59 (2005).

[102] J.-P. Mulet, K. Joulain, R. Carminati, and J.-J. Greffet, Enhanced radiative heat transfer at nanometric distances, Microscale Thermophys. Eng. **6**, 209 (2002).

[103] E. Rousseau, A. Siria, G. Jourdan, S. Volz, F. Comin, J. Chevrier, and J.-J. Greffet, Radiative heat transfer at the nanoscale, Nat. Photonics **3**, 514 (2009).

[104] D. Barchiesi and T. Grosges, Fitting the optical constants of gold, silver, chromium, titanium, and aluminum in the visible bandwidth, J. Nanophotonics **8**, 083097 (2014).